The Thesis committee for Sagi Zisman
Certifies that this is the approved version of the following thesis:

Multiple-Input Multiple-Output (MIMO) for Multimode Optical Fiber Communication Channels

APPROVED BY

SUPERVISING COMMITTEE:

Sriram Vishwanath, Supervisor

Seth Bank

Multiple-Input Multiple-Output (MIMO) for Multimode Optical Fiber Communication Channels

by

Sagi Zisman, B.S.E.E.

THESIS

Presented to the Faculty of the Graduate School of

The University of Texas at Austin

in Partial Fulfillment

of the Requirements

for the Degree of

MASTER OF SCIENCE IN ENGINEERING

THE UNIVERSITY OF TEXAS AT AUSTIN

December 2012

Dedicated to my parents Dalia and Ilan.

Acknowledgments

This is perhaps the most important section of this thesis. I wish to shed light and thank the people whose support has kept me going in my quest for knowledge, and more concretely, have enabled the research in this project. First and foremost, I would like to thank my co-advisors Dr. Sriram Vishwanath and Dr. Seth Bank for providing me the opportunity, and support (both scholastically and financially) to engage in research in optical communications. While the journey wasn't always smooth, I appreciate the push and the confidence you had in me to succeed. I would like to thank my friend (and collaborator) Kumar Appaiah for being a true mentor and without a doubt, one of the most knowledgeable, helpful, and fun people I have ever met. The knowledge of MIMO systems that you taught me has been tremendously helpful for the project; your quirkiness made working much more enjoyable. Most importantly though, it was the support of my parents, brother, and sister that got me to this point. Through thick and thin, your encouragement and enduring love have kept me going. Finally, I would like to thank my girlfriend Natalie Zeldin for enforcing a strict pacing regimen that saw me finishing the writing earlier and on schedule. Without you, I would probably have done this thesis in the last week, with infinite stress, and it would not nearly be as good. I love you.

Multiple-Input Multiple-Output (MIMO) for Multimode Optical Fiber Communication Channels

Sagi Zisman, M.S.E.
The University of Texas at Austin, 2012

Supervisor: Sriram Vishwanath

This thesis evaluates the benefits of Multiple Input Multiple Output (MIMO) techniques on the capacity of Multimode Fiber (MMF) links. Optical MMF MIMO systems take advantage of the spatial diversity present in the multiple propagating paths in multimode fibers. By using multiple lasers at the input facet of the fiber and multiple photodetectors at the output, we show that the capacity of the link is improved from the single device link, hence demonstrating the usefulness of MIMO in such optical systems. An initial simulation of butt-coupling a Vertical Cavity Surface Emitting Laser (VCSEL) to multimode fiber reveals that the placement position of the laser axis with respect to the fiber axis is critical in exciting a large number of modes. More specifically, we show that there exists a tradeoff between total power coupled into the fiber and the number of modes launched. We then consider a mathematical description of the fiber channel and use it to simulate the capacity of a 1×1, 2×2, and 3×3 MIMO links over a statistical ensemble of channel realizations. This simulation reveals that a 2×2 system is capable of approximately a 50% increase in capacity over the 1×1 case while the 3×3 system is capable of approximately an 80%

increase. Moreover, we show that the choice of the placement positions on the facets of the fiber affects the channel capacity, thereby implying that an optimal device position exists. We find the optimal device geometry by an exhaustive search and compare the capacities for the optimal geometry and that of a suboptimal one. A capacity tolerance study is then developed that considers perturbations about the optimal device locations and shows that the capacity of a rotated laser plane is over 90% of the capacity of the original device locations. A second perturbation study considers lateral offsets and shows that systems with a higher number of devices show good tolerance with poorer lateral tolerances for systems with less devices. When small lasers and a large grid of possible device locations are used, an exhaustive search for the optimal device location becomes computationally infeasible. We show that the problem of searching for the optimal detector locations while holding the laser positions fixed is submodular. This property allows a greedy algorithm to select the device positions at a small fraction of the computational complexity, however, only guaranteeing that the capacity of the resulting configuration is greater than a $(1 - e^{-1})$ fraction of the optimal configuration. We use this technique to compare the exhaustive search and the greedy search for coarse grids, and then exclusively use the greedy algorithm to select a device configuration for a fine grid whereby an exhaustive search is computationally infeasible.

Table of Contents

List of Figures

Chapter 1

Introduction

The goal of a communication system is twofold. One is to send as much data from a sender to a receiver as possible in the least possible amount of time, called the data rate through the system. Two, it should occur with as small a number of errors as possible, called the error rate. Back in the mid part of twentieth century, Claude Shannon showed mathematically that communication over noisy channels is possible with an arbitrarily small probability of error with a data rate that is called the capacity of the channel [1]. This data rate is to be interpreted as the highest theoretical rate possible when requiring no errors. In practice, the data rates are lower. A large part of research in communication systems deals with increasing the capacity of the channel. To that end, one technique that has been formulated is termed Multiple Input Multiple Output (MIMO) communication [2]. The premise and hence usefulness of MIMO rests on the fact that it introduces a diversity gain [3]. This diversity gain has been shown to increase the data rates in wireless systems [2]. There are various ways to introduce the diversity gain. One such way is termed spatial gain [3]. Intuitively, it increases the data rate by using multiple independent spatial paths to transmit the data. If one path is too noisy, the other ones can be used to detect the information instead. This spatial gain can be implemented by using multiple transmit and multiple receive antennas which give rise to the name Multiple Input Multiple Output [3].

With the increasing global demand for bandwidth, the preferred medium of communication for long distances and more recently, that of high-speed short distance links is the fiber optic cable. As always, the capacity of the communication channel should be maximized. An interesting question arises. If in wireless systems the use of multiple transmitter and receiver antennas is shown to increase the capacity, does a similar increase in capacity follow for fiber optic channels when multiple lasers (transmitters) and photodetectors (receivers) are used? If so, by how much is the capacity increased (in comparison to the one laser and one photodetector system)? What degrees of freedom are available to us and how do we select their optimal values that maximize the capacity? This thesis will explore the answers to these questions in detail and will illuminate the usefulness of MIMO for fiber optic channels. More specifically, when using multiple transmitters and receivers, it is reasonable to ask how to place them with respect to the input and output of the optical fiber. Through simulations, this thesis will argue that this question becomes a central theme and is critically important for maximizing the capacity of the channel.

This thesis is broken down into six chapters. Chapter 2 covers background information that is needed to understand the rest of the thesis. In particular, it covers basic MIMO concepts and introduces the important notion of guided modes in multimode fibers. Chapter 3 talks about an initial study designed to learn the parameters and the placement of one laser at the input of a multimode fiber that maximizes the spatial diversity of the channel upon launch without worrying about the details of how light travels in the fiber and all the associated complexities. Chapter 4 dives headfirst into a systematic simulation and calculation of channel capacities based on a probabilistic fiber channel model found in the literature. This chapter is the meat of this thesis and will illustrate and give proof to

the central theme, i.e. that the placement position of lasers and detectors critically affects the capacity of the channel. For a few examples, it will give these optimal placement positions, however, at the cost of painful computational complexity. Chapter 5 mitigates the computational complexity by showing that by fixing a laser configuration at the input, the photodetector configuration at the output obeys the submodularity property, hence, a greedy algorithm can be used at a fraction of the computational cost. However, a tradeoff exists, namely, that the greedy method cannot be guaranteed to yield the optimal placement all the time, but instead, guarantees a "sufficient" placement. Chapter 6 will proceed to conclude the thesis.

Chapter 2

Background Information

2.1 Multimode Fibers

MIMO relies on the concept of diversity gain to increase the capacity through the channel. In particular, it takes advantage of spatial diversity, that is, multiple independent paths through the channel. In fiber optics, this naturally translates to the multiple propagating modes that are afforded by multimode fiber (MMF). Each propagating mode corresponds to a different physical path through the channel. In order to use these modes for spatial diversity, we need to know how to activate them, or in other words, how to excite them. An excitation occurs when light from a source (such as a laser) is incident on the fiber. One way to do this is by butt-coupling, meaning, that the light source is simply placed (commonly with special glue) on the input facet of the fiber with the output plane of the laser on the input plane of the fiber. Another technique to excite fiber uses a lens to focus the light from a source onto the fiber input. This thesis uses the butt-coupling technique, mainly in order to reduce simulation complexity. To take advantage of diversity, we would like a large number of modes to be excited. How can we predict which modes get excited? The following two sections will describe mathematically the modes of MMF and the notion of excitation. Armed with the mathematics, we will be in a position to predict (simulate) the modes that are excited.

2.1.1 MMF Modes

Light, being an electromagnetic phenomenon, is governed by Maxwell's Equations. The equations form a set of four differential vector equations that must be solved simultaneously. Generally, boundary conditions are specified for the field quantities and the equations solved; dielectric interfaces are the spatial locations defining the boundaries. Therefore, different geometrical dielectric structures will yield different solutions. Optical fibers are generally of cylindrical geometry. They have a core cylinder wrapped in a cladding cylinder whereby the index of refraction of the core is higher than the cladding. To attempt a solution, we first write Maxwell's equations in a source free region [4]:

$$\begin{array}{ll} \nabla \bullet \mathbf{E} = 0 & \nabla \times \mathbf{E} = -\frac{\partial \mathbf{B}}{\partial t} \\ \nabla \bullet \mathbf{B} = 0 & \nabla \times \mathbf{B} = \mu(\mathbf{r})\epsilon(\mathbf{r})\frac{\partial \mathbf{E}}{\partial t} \end{array} \tag{2.1}$$

Taking the curl of the curl of the electric field, switching the order of the spatial derivative ∇ and the time derivative, and substituting the curl of the magnetic field yields the well-known Helmholtz equation [4]:

$$\nabla^2 \mathbf{E} = \mu(\mathbf{r})\epsilon(\mathbf{r})\frac{\partial^2 \mathbf{E}}{\partial t^2} \tag{2.2}$$

This differential equation is in fact three differential equations, one for each component of the electric field. We will consider solutions to the scalar wave-equation whereby one electric field component is selected. Solving for the time-dependence of the electric field is easy. Employing the method of separation of variables, $E(\mathbf{r}, t) = u(\mathbf{r})g(t)$ and letting the separation constant be $-\omega^2$, we get a time-dependence of $g(t) = e^{-i\omega t}$. Plugging $E(\mathbf{r}, t) = u(\mathbf{r})e^{-i\omega t}$ back into Eq. 2.2, the time-dependence falls out and noticing that $\mu\epsilon = \frac{1}{v^2}$ where v is the velocity of the wave, $n = \frac{c}{v}$, $c = \frac{\omega}{k}$, $k = \frac{2\pi}{\lambda}$ where λ is the free-space wavelength, the

time-independent wave equation becomes:

$$(\nabla^2 + k^2 n^2(\mathbf{r}))u(\mathbf{r}) = 0 \tag{2.3}$$

This equation is now purely a differential equation in space whose solutions are allowed spatial electric field profiles. For different dielectric structures, the index of refraction function $n(\mathbf{r})$ changes and potentially changes the set of solutions to the equation. Specifically, for cylindrical dielectric structures of concern to us here, the index of refraction takes the form [5]:

$$n^2(\mathbf{r}) = \begin{cases} n_{core}^2 - (ar)^2 & r \leq R \\ n_{clad}^2 & r > R \end{cases} \tag{2.4}$$

In this equation R is the core radius of the fiber, and n_{core} and n_{clad} are the core and cladding index of refraction respectively. To ensure continuity of this function across the core-cladding boundary, the constant $a = \frac{n_{core}^2 - n_{clad}^2}{R^2}$. Note that within the core region, a parabolic index of refraction fall-off is present. An optical fiber with this type of profile is called a graded-index fiber. The reason for a graded-index is to mitigate the effects of modal dispersion. Modal dispersion will be discussed later after the fiber modes are introduced. Solving Eq. 2.3 with the above index profile is a formidable task. Many papers exist discussing the solution of the Helmholtz equation for various geometries and with various degrees of mathematical complexity. One such paper that attempts to solve the wave equation with a parabolic index of refraction, and which this thesis will follow in the following discussion is given in [5]. As an approximation, to help ensure an analytic solution, $R \to \infty$. The cylindrical optical fiber is azimuthally symmetric, meaning that the electric field amplitude depends only on the radial distance to the central fiber axis. With this information, the azimuthal dependence

of the spatial profile can be extracted to yield:

$$\hat{u}(\mathbf{r}) = u(r, z)e^{-i\nu\phi} \tag{2.5}$$

In this equation, ν must be an integer to ensure that the phases match up after a 2π rotation. This intuitively leads to the azimuthal mode number. The mathematical details of solving the rest of the differential equation are of little interest here, and hence, the final form is found from [5] to be:

$$\hat{u}_{\mu\nu}(\mathbf{r}) = N * r^{\nu} L_{\mu}^{\nu}(kar^2) \exp[i\nu\phi + ikR(z) - kar^2/2] \tag{2.6}$$

In this equation, L_{μ}^{ν} is the well-known Laguerre polynomial where μ is the radial mode number and ν is the azimuthal mode number. N is a proportionality constant that can be set by requiring some normalization of power. It is interesting to note the exponential factor at the end of this expression. The first term in the exponential gives a linear phase accrual in the azimuthal coordinate. The second term gives a phase accrual in the longitudinal direction governed by the function $R(z)$. The third term is a Gaussian amplitude decay when moving radially from the central fiber axis. The Gaussian amplitude decay along with the Laguerre polynomial give rise to the name Gauss-Laguerre modes. For each integral value of μ and ν, a different electric field profile is realized, and thus gives rise to the different modes of a dielectric structure.

The above discussion was meant to justify the origins of the modes in an optical fiber and their emergence as the solutions to the Helmholtz equation. A more tractable mathematical description of the modes with an illuminating physical discussion is given in

"*Lasers*" by Siegman as [6]:

$$\tilde{u}_{pm}(r,\theta,z) = \sqrt{\frac{2p!}{(1+\delta_{0m})\pi(m+p)!}} \frac{\exp\ i(2p+m+1)(\psi(z)-\psi_0)}{w(z)} (\frac{\sqrt{(}2)r}{w(z)})^m L_p^m (\frac{2r^2}{w(z)^2}) \\ * \exp(-ik\frac{r^2}{2\tilde{q}(z)} + im\theta) \quad (2.7)$$

In this equation, p is the radial mode number while m is the azimuthal mode number. The factor given by $\frac{\exp\ i(2p+m+1)(\psi(z)-\psi_0)}{w(z)}$ represents the phase accumulation along the longitudinal axis. For the purposes of the simulations in this thesis, the assumption is that the field profiles are sampled at what is termed the beam waist. The beam waist is found by setting $z = 0$. The longitudinal phase factor then drops out because $\psi(z) = \psi_0$. The quantity given by $w(z)$ is called the beam spot size and is a measure of the thickness of the beam (its radius) at a particular longitudinal coordinate.

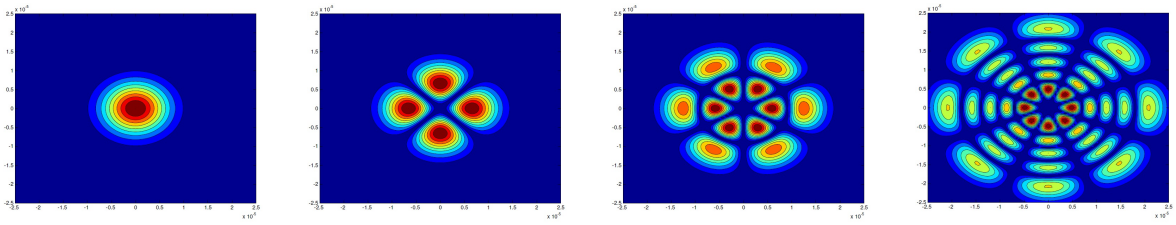

(a) (b) (c) (d)

Figure 2.1: Intensity profiles for the modes (a) p = 0, l = 0, (b) p = 0, l = 2, (c) p = 1, l = 3, (d) p = 4, l = 4

A MATLAB routine that plots the amplitude of the above field is written for the purpose of verifying the correct mathematical expression. Figure 2.1 shows the intensity plots of the fundamental mode and various higher order modes.

2.1.2 Overlap Integral and Coupling Coefficients

The Helmholtz equation is a linear partial differential equation. This implies that linear combinations of its solutions must also satisfy the equation. The solution set of the Helmholtz equation can be generalized as a complete inner product space over the set of complex numbers. This space is sometimes referred to as Hilbert Space [7]. The modes given above form a complete orthogonal basis set for the space that can then be used to span the space. This means that any function can be written as a linear combination of the Gauss-Laguerre modes with complex coefficients. Sometimes the modes are called the eigenmodes of the dielectric structure because they form the natural basis set for the particular geometry. Let $f(r,\theta,\phi)$ be an arbitrary complex function that approaches zero as the radial coordinate is taken to infinity, and $GL_{p,m}(r,\theta,\phi)$ the Gauss-Laguerre function of order {p,m} as defined explicitly in Eq. 2.7, then,

$$f(r,\theta,\phi) = \sum_{p,m} \tilde{c}_{p,m} GL_{p,m}(r,\theta,\phi) \tag{2.8}$$

The inner product of two elements, say f and g, for this function space is defined as an "overlap integral" given by:

$$< f|g >= \int f^*(r,\theta,\phi) g(r,\theta,\phi) d\mathbf{r} \tag{2.9}$$

The expansion coefficient of an arbitrary function f in the basis of Gauss-Laguerre modes is then given by:

$$\tilde{c}_{p,m} =< GL_{p,m}|f > \tag{2.10}$$

Thus, associated with each complex function is a vector of complex coefficients in the basis of the Gauss-Laguerre modes.

We can define a "coupling coefficient" between an electric field profile and a particular eigenmode of the fiber as the intensity contained in a particular eigenmode of the fiber in the expansion of the incident light (from henceforth, laser light) field normalized to the product of total intensities of the incident field and the fiber eigenmode [8]. That is, let $\eta_{p,m}(f_{\text{Laser}})$ be the coupling coefficient between the incident laser field and the {p,m} mode of the fiber. Generally, it is a function of the input laser electric field profile. Then,

$$\eta_{p,m}(f_{\text{Laser}}) = \frac{|< GL_{p,m}^{\text{fiber}}|f_{\text{Laser}}>|^2}{|< f_{\text{Laser}}|f_{\text{Laser}}>|^2 * |< GL_{p,m}^{\text{fiber}}|GL_{p,m}^{\text{fiber}}|^2} \tag{2.11}$$

2.1.3 Waveguide Perturbations and Modal Dispersion

In an ideal waveguide, with a perfect dielectric structure, the vector representing an electric field profile remains unchanged while propagating through the waveguide. However, if there are any dielectric imperfections, the Gauss-Laguerre modes are no longer the eigenmodes of that imperfect section of the waveguide. What ends up happening is a transformation of the original vector into another as it enters the imperfect section of the waveguide. This can be modeled as a matrix transformation that will be described in a later section.

When dealing with a three-dimensional structure, phase will generally not be accrued equally in all three dimensions. As a simple example, a plane wave can be envisioned whereby points on the wave front are equiphase points. Boundary conditions in each dimension will determine how the phase is accrued. Combining the three dimensions together, we get what is called the wave vector **K** that points in some direction. The higher the mode of the fiber, the greater the angle this vector will make with the central fiber axis. This means that the higher order modes "bounce" off the edges more often than the lower-order modes. This implies that the higher-order modes take a longer time to traverse the length of the fiber

since they cover more distance. This effect is called *modal dispersion*. To mitigate this effect, the fiber is made graded, that is, the index of refraction decreases from the central fiber axis. This allows the waves that are traveling on longer trajectories through the fiber to speed up. This effect equalizes the optical path length of the modes such that they arrive at the output of the fiber at the same time and preserves signal quality. Recalling Eq. 2.4, it can be seen that indeed the index of refraction falls off in a quadratic fashion from the central axis of the fiber.

2.2 Basic MIMO Concepts

As described in Chapter 1, MIMO uses multiple transmit and receive elements to increase the capacity of the channel by taking advantage of *diversity gain*. Diversity gain is the benefit that is derived from using multiple independent paths to transmit the signal across the channel. One way to accomplish this diversity is by using different spatial paths that transform the signal independently across the channel. It can now be imagined that the spatial orthogonal eigenmodes of the optical fiber fulfill this requirement. This thesis rests precisely on this crucial point. The higher the number of independent paths, the higher the potential data rate. Associated with a MIMO channel is a matrix called the system matrix, denoted as $\mathbf{H}$, of dimension $N_R \times N_T$ where N_R is the number of receivers of the system and N_T is the number of transmitters of the system. The elements $[H]_{ij}$ of this matrix correspond to the different paths through the channel and give the gain of the path associated with the j^{th} transmitter and i^{th} receiver. For the technique to be useful, the elements of this matrix should be independent and uncorrelated in order to increase the ergodic capacity of the channel [9].

The calculation of the system matrix is dependent on the implementation of the channel and will be described in Section 4.2. However, a useful conjecture can be thought. If light is launched into as many modes as possible, specifically, that each transmitter will launch into a distinct set of modes, and each mode transforms independently through the channel, then the likelihood that the gains of each particular link, say that between the j^{th} transmitter and i^{th} receiver, are independent and uncorrelated is higher [10]. In essence, without really knowing the transformation that the channel imposes, we at least know that the number (diversity) of modes upon launch should be high. This leads us to an initial study in Chapter 3 to learn how light couples into an optical fiber and what modes are excited upon launch with an eye towards increasing this number of modes.

Chapter 3

Initial Study on Modal Excitation

As described in Section 2.2, launching light or exciting the optical fiber into a large number of modes increases the likelihood of having independent, uncorrelated entries to the MIMO system matrix. To investigate how this can best be done, a MATLAB simulation is conducted that uses one laser, for example, a Vertical Cavity Surface Emitting Laser (VCSEL), to excite a MMF with a butt-coupling scheme. The goal is to figure out what parameters and degrees of freedom give us the highest possible number of modes upon launch. To calculate what fraction of the power of the incident light is coupled into each fiber mode, Eq. 2.11 is used. It should be noted that the inner products in the equation are integrals over space. This means that the relative positions of the incident electric field profile and the profile of the fiber modes are of prime importance. Intuitively, the more they overlap, the higher the fraction of incident power that is coupled into the mode. This tells us that as the laser axis is offset from the central fiber axis, different sets of modes will be excited. What is the best offset that will give us a large number of modes and that will allow most of the power to couple into the fiber in the first place? The incident light field, and hence its overlap with the fiber, also depends on the size of the laser. What happens when the laser size is modified? These are some of the questions that this chapter aims to answer.

It is important to bear in mind that this study does not give quantitative or even

incisive results in regards to the capacity of the fiber link, but merely illuminates interesting features of the launch diversity and the conditions that increase this diversity[1]. This chapter describes the simplistic model that was used to simulate both the laser and the fiber including parameters used, a few graphs highlighting important trends for various cases and shows that there is generally a tradeoff between the number of modes that are excited and the total power carried by the guided modes.

3.1 Simplistic Laser and Fiber Model

The model used for the fiber is a simple cylindrical shape with a core and a cladding. For simplicity, the laser is also taken to be of the same geometry and to possess the same parameters as the fiber, that is, the problem is equivalent to coupling light from one fiber to another. The physical connection between the laser and the fiber was assumed to be a butt-couple. To calculate how light excites the fiber, all that needs to be done is to take the output electric field profile from the laser, and using the overlap integral, calculate all the coupling coefficients to the various modes. This means that free-space propagation or other optical coupling instruments can be ignored. The important parameters and equations that are used in the simulation are those found in a paper titled "Butt-Coupling Efficiency of VCSEL's into Multimode Fibers" by J. Heinrich *et al.* [8]. In this paper, Heinrich compared two types of lasers, an oxidized VCSEL and a proton-implanted VCSEL, to see which couples more efficiently into a graded MMF. Heinrich found that the proton-implanted laser gives a larger coupling efficiency that is nearly independent of laser driving current and above 80% [8].

[1] In fact, there might be roundoff errors or discretization errors from numerical calculations that yield results that may not obey conservation of energy. The numerical results are understood to be approximate. In any case, the qualitative results hold.

This observation can be useful for our research when the lasers we use for the MIMO system need to be fabricated. Heinrich then develops a theoretical model that predicts the coupling coefficients into various modes given the relative laser/fiber sizes and relative laser/fiber index of refraction differences (difference between core and cladding). Our initial study borrows the theoretical model for the parameters developed by Heinrich, with the important additional capability of offsetting the laser and fiber central axes relative to each other. This additional capability allows us to study possible placement locations for the lasers in our MIMO system.

3.1.1 Simple Model Parameters

According to [8], the parameters to use in the coupling coefficient study using the simplistic model are the laser and fiber core diameters, the index of refraction profiles of the laser and fiber, the index of refraction difference between the core and the cladding, the wavelength of light, and the mode at which the laser operates (assumption is that the laser outputs only one mode). The index of refraction functional dependence on the radial distance from the fiber central axis is the quadratic fall-off given by [8]:

$$n_L(r) = n_{oL} - \tilde{n}_L r^2/2 \tag{3.1}$$

The parameter $\tilde{n}_L = \frac{8\Delta n_L}{d_L^2}$ where d_L represents the "active" laser diameter. n_{oL} is the on-axis index of refraction of the laser, and Δn_L is the on-axis and core index of refraction difference. Similar expressions hold for the fiber indices of refraction where the above subscripts are replaced from "L" by the letter "F". Finally, the field radius that represents the radius of

the electric field intensity for the modes of the laser and fiber can be given by [8]:

$$w_L = \sqrt{\frac{\lambda d_L}{2\pi\sqrt{2n_{oL}\Delta n_L}}} \tag{3.2}$$

In this particular simulation, the field radius, w, is taken to be the beam waist size such that the output of the VCSEL butt-coupled to the fiber will be incident at its waist on the fiber endface. For a wavelength of $\lambda = 1550$ nm, $d_F = 50$ μm diameter fiber, a fiber core index of refraction $n_{oF} = 1.5$, and a refractive index difference of $\Delta n_F = .015$ between core and cladding results in a field radius $w_F = 7.625$ μm using equation 3.2. These characteristic numbers are used as in [8]. Now, in the simulation, the mode field radius of the laser, w_L, is used as a variable.

Another degree of freedom includes the particular laser mode that we are interested in coupling into the fiber. This mode is given by two indices, p_{laser} in the radial direction, and l_{laser} in the azimuthal direction that index the laser modes. Generally speaking, a single mode laser will operate in the fundamental mode (such as the ones in our lab). Depending on the particular simulation we want to run, the fiber mode indices p_{fiber} and l_{fiber} can also be specified or used as variables. More will be said about these parameters in the subsequent sections.

A final note on coupling efficiency from a laser to a multimode fiber is in order. We are interested in the excitation of guided fiber modes because only the guided modes are useful paths which can be used for communication purposes. Any unguided mode represents energy that is lost to the cladding of the fiber. To determine the modes that are guided in the fiber, we can use the formula that is given by [8]:

$$\tilde{l}_{\max} = \text{int}\left(\frac{\pi d_F}{2\lambda}\text{NA}\right) \tag{3.3}$$

$$\tilde{p}_{\max} = \text{int}\left(\frac{\pi d_F}{4\lambda}\text{NA} + \frac{1}{2}\right) \tag{3.4}$$

The variable NA is the numerical aperture of the fiber and can be computed by the following equation [8]:

$$\text{NA} = \sqrt{2n_{oF}\Delta n_F - \Delta n_F^2} \tag{3.5}$$

Using $n_{oF} = 1.5$, $\Delta n_F = .015$, we get NA = .21. Plugging in the numerical aperture along with $\lambda = 1550$ nm and $d_F = 50$ µm into Eqs. 3.3 and 3.4, where the *int* operation is taken as the floor operator, we get $\tilde{p}_{\max} = 5$ and $\tilde{l}_{\max} = 10$. These formulas determine the maximum mode number for the radial and azimuthal modes that are guided. In [8], the lowest radial number starts at one and the lowest azimuthal number starts at zero, whereas in our simulation, the lowest radial number starts at zero. This is largely a matter of convention as long as the two yield the same set of guided modes. Hence, our simulation allows $\tilde{p}_{\max} : 0 \to 4$, and $\tilde{l}_{\max} : 0 \to 10$.

3.1.2 Simple Model Simulation

The MATLAB simulation consists of the calculation of coupling coefficients into the guided fiber modes for different variable values as laser/fiber relative sizes, different laser mode numbers, and most importantly, for different radial offsets. Since the coupling coefficients give the fraction of total power contained in a particular mode, they can be used to determine the number of modes that contribute to the spatial diversity requirement. For example, we can say that any guided mode that contains 1% of incoming power (equivalently, with the associated coupling coefficient) contributes to the diversity. These modes can then be added up to give the total diversity count for a set of parameters. Then, we can compare

across different sets of parameters to choose the one that yields the highest diversity count.

We begin by taking an x-y plane of dimensions -25 μm to 25 μm in both the x and y direction. The plane is discretized into a grid with a step size of .5 μm. This grid will be used to define the electric field profile functions spatially and is the plane of incidence of the laser output onto the fiber input and acts as the overlap plane. Both the laser and the fiber are assumed to be at the beam waists at this plane. The scalar electric field profile is given in Eq. 2.7 and both the laser and fiber profiles are assumed to be polarized in the same direction for simplicity. The fiber beam (mode) size to use in the equation ($w(0)$) is calculated above (section 3.1.1) as $w_F = 7.625$ μm and the central position of the profile on the overlap plane is a variable to be varied by a coordinate-shift of x and y in Eq. 2.7. The mode numbers are also specified in this equation and are variables.

3.2 Modal Excitation Results

As stated at the beginning of this chapter, the goal is to determine conditions that increase the number modes excited upon launch. In the lab, it is likely that single mode VCSELs operating in the fundamental mode ($p = 0, l = 0$) will be used. A good first test fixes the laser to the fundamental mode and matches the laser and fiber mode field radii to $w_F = w_L = 7.625$ μm. Then, the laser is offset radially and the coupling coefficients are calculated. Figure 3.1 shows the coupling coefficients for the $p = 0$ fiber modes. It can be seen that when the laser is perfectly centered with the fiber ($r = 0$), the coupling coefficient from the fixed laser mode $p = 0, l = 0$ to the fiber mode $p = 0, l = 0$ is 1 as expected. In the language of linear algebra, since the input laser mode electric field function is equal to that of the fiber (equivalent mode numbers, mode radii, and centered perfectly),

in the expansion of the fundamental laser mode electric field function in the eigenmodes of the fiber, only the fundamental mode of the fiber is used whereas all other modes are not used. Thus, the other coupling coefficients are zero, again, as expected. As the laser is offset, contributions from other modes begin to emerge in a sequentially increasing azimuthal order, while the contribution of the fundamental mode decays. This might lead us to conclude that somewhere between 10 μm and 15 μm is the best operating offset.

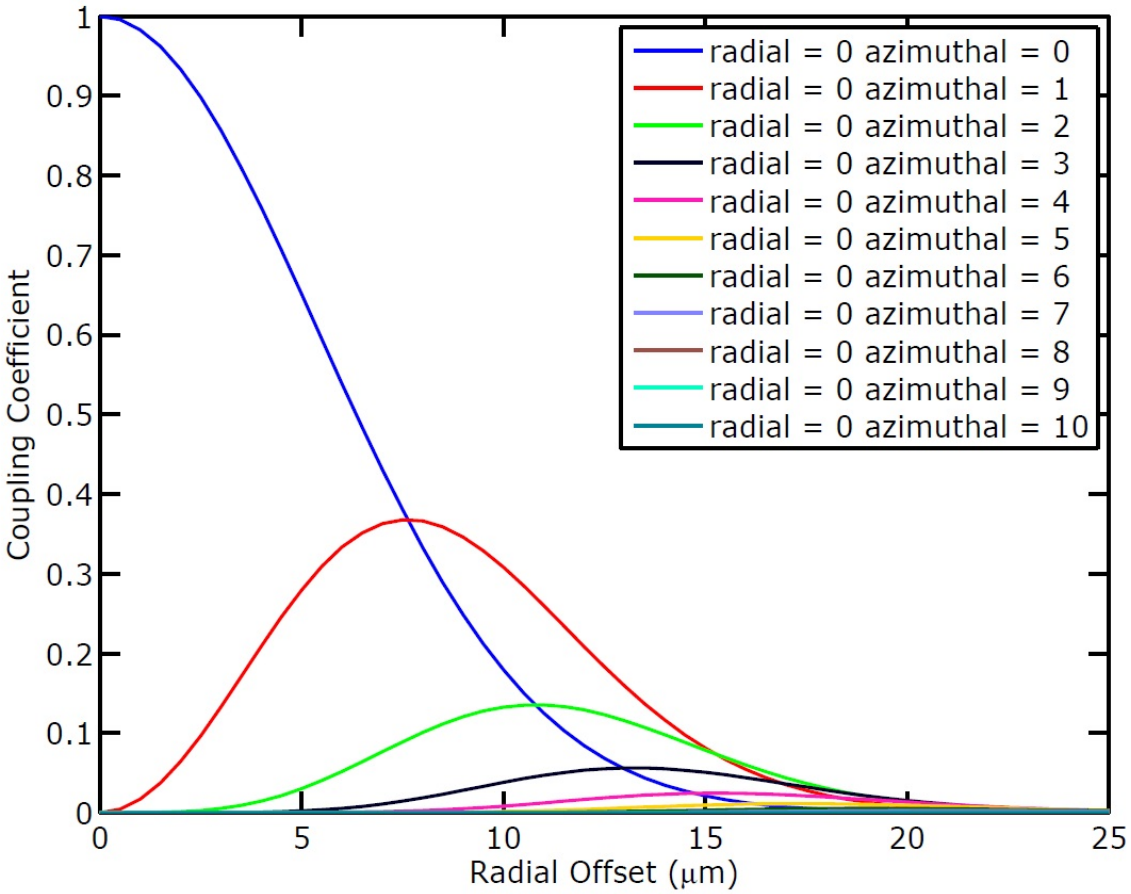

Figure 3.1: Coupling of p = 0, l = 0 laser mode to various fiber guided modes as a function of radial offset

However, the problem with Figure 3.1 is that it only looks at the $p = 0$ guided modes. Recall that the maximum radial number for the fiber is 4. Other modes which have not been plotted also have a contribution. A better metric to consider is summing up the total number of modes above a certain coupling coefficient threshold for a given set of parameters (laser mode and size). This will facilitate easier comparison between sets of parameters and segment the parameter space more compactly. To that end, we consider a laser operating in the fundamental mode being coupled to a $w_F = 7.625$ µm fiber for laser sizes of $1, 3, 5, 7.625, 10, 15$ µm. The idea is to find the optimal laser size and radial offset that yields the highest number of modes with a coupling coefficient of $\geq 1\%$. Figure 3.2 graphs the number of modes activated for the given laser sizes.

From the plot, it is seen that the highest number of modes are attributed to the 5 µm, or the 3 µm mode field laser size at an approximate offset of about 20 µm. The exact value is 27 modes at 20 µm offset for the 5 µm laser. The curve shows us an increasing trend in the number of modes activated as a function of the radial offset, and at large offsets, the smaller the laser size, the higher the number of modes that is excited. One notable exception is the smallest laser size, 1 µm, that quickly falls off and hits zero modes for an offset of 21 µm. This is due to the fact that the smaller the size of the laser modal field, the faster its overlap with the fiber modes diminish and past a certain point, there will be negligible overlap. What if only the modes with $\geq 5\%$ coupling efficiency are useful for the diversity requirement? Attenuation and intermodal coupling affect to diminish the power in any particular mode, therefore, it becomes important to consider the power that is carried by the modes as well. Using the same parameters as those used in Figure 3.2, but counting only modes with $\geq 5\%$ coupling efficiency, we get Figure 3.3. In this plot, the highest number of modes is 9 where

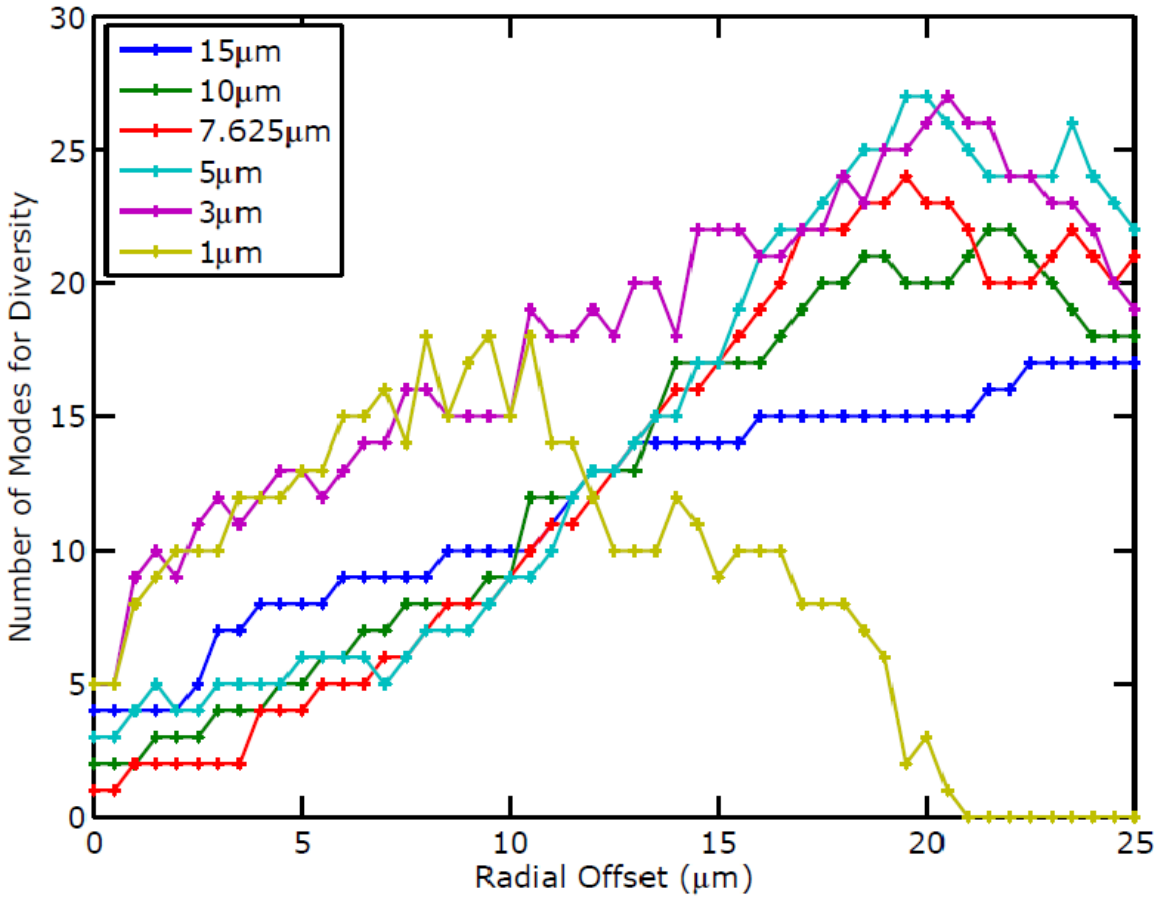

Figure 3.2: Total number of guided modes with a coupling of $\geq 1\%$ from a $p = 0, l = 0$ laser mode and various laser sizes as a function of radial offset

all but the 1 µm and 3 µm laser excite this number of modes. This maximal excitation occurs for the 5 µm and 7.625 µm at around $13 - 14$ µm radial offset. The larger laser sizes hit 9 excited modes later around $18 - 20$ µm radial offset. Comparing Figure 3.2 to Figure 3.3, we see that the highest number of modes seem to occur for smaller laser sizes, but the majority of such modes possess less than 5% of the incident power, whereas the larger laser sizes support a fewer number of modes, yet the fraction of modes with $\geq 5\%$ power is

much larger. Clearly, the laser size that should be used depends on how much power each mode needs to carry to be useful in MIMO and will depend on the particular channel.

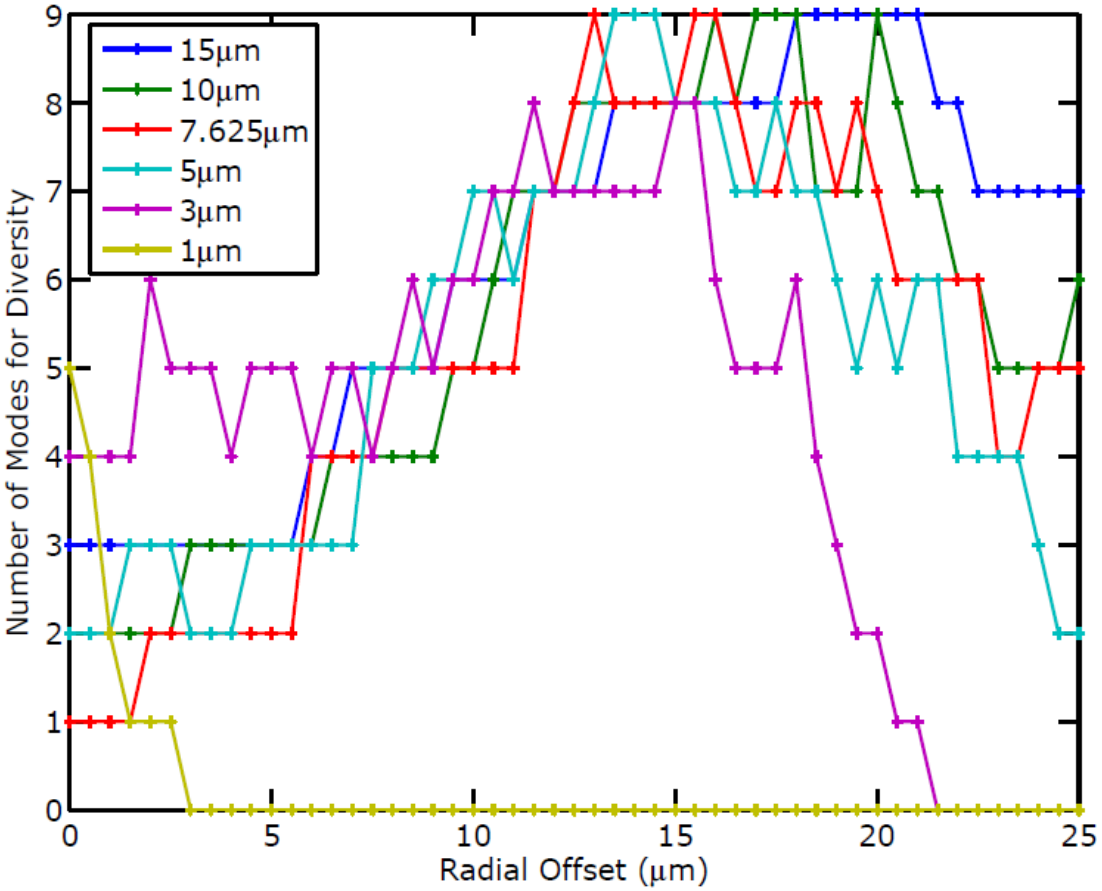

Figure 3.3: Total number of guided modes with a coupling of $\geq 5\%$ from a $p = 0, l = 0$ laser mode and various laser sizes as a function of radial offset

The number of modes that are excited in a channel is not the only important measure to consider in a communication system. The Signal to Noise Ratio (SNR) is higher when the power of the signal through the channel is higher. It is imperative to couple enough power into the guided modes in the first place. How much power gets coupled into the guided

modes? Using the same parameters as the above plots, namely, laser modes $p = 0$, $l = 0$, and fiber active diameter $w_F = 7.625$ µm, Figure 3.4 shows the total power that is coupled into the fiber for each of various laser mode field sizes as the laser is offset from the central position. As the radial offset is increased, the total coupling into the guided modes of the

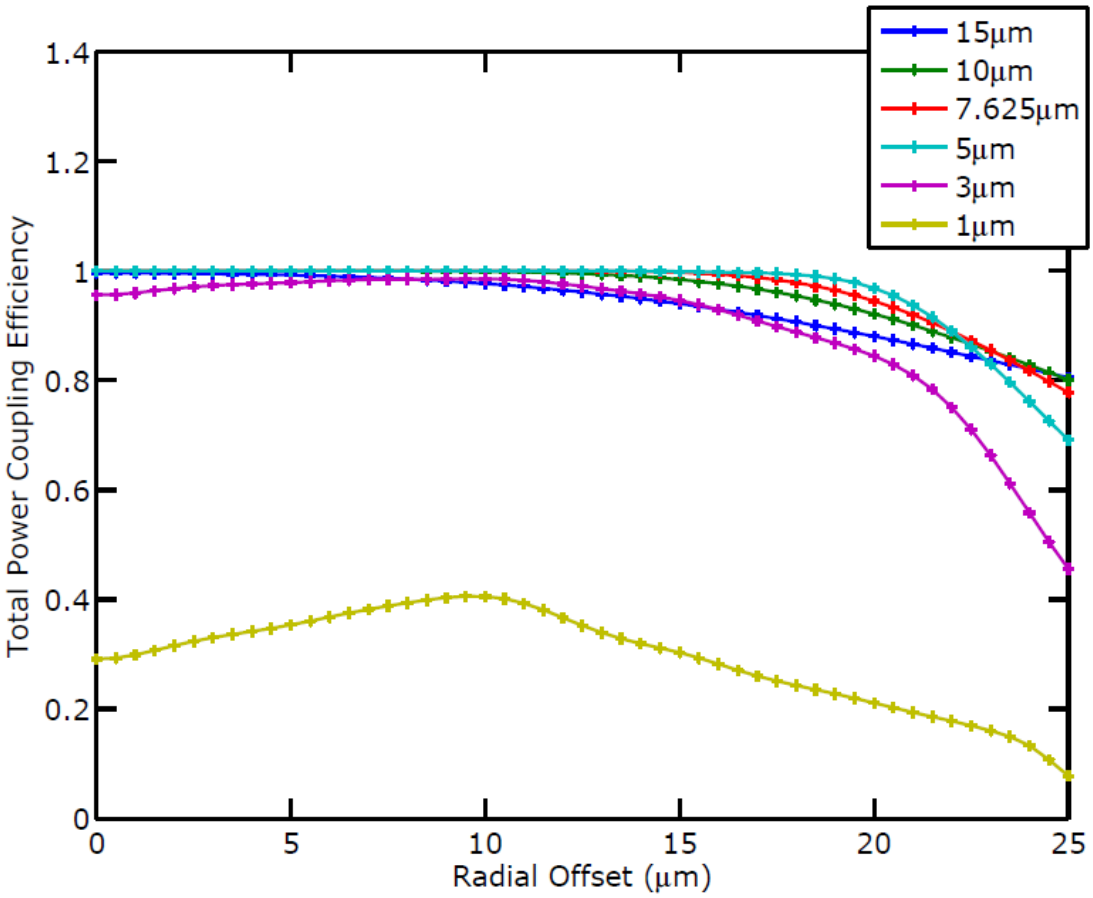

Figure 3.4: Total power coupled into guided modes from a p = 0, l = 0 laser for various laser sizes as a function of radial offset

fiber generally decreases. This can be attributed to the fact that at some offset position, the laser and fiber are not fully overlapping. Recall that the active fiber diameter is 50

μm and therefore, at an offset of 25 μm, a laser is only partially overlapping the fiber and some of the light is not coupled into the fiber; this is simulating offsetting the laser past the physical edge of the fiber. The sharper drops occur for the smaller size lasers. This is due to the fact that the overlap diminishes at a smaller offset when the laser mode field size is smaller. Moreover, out of the guided modes, if only the guided modes over a certain

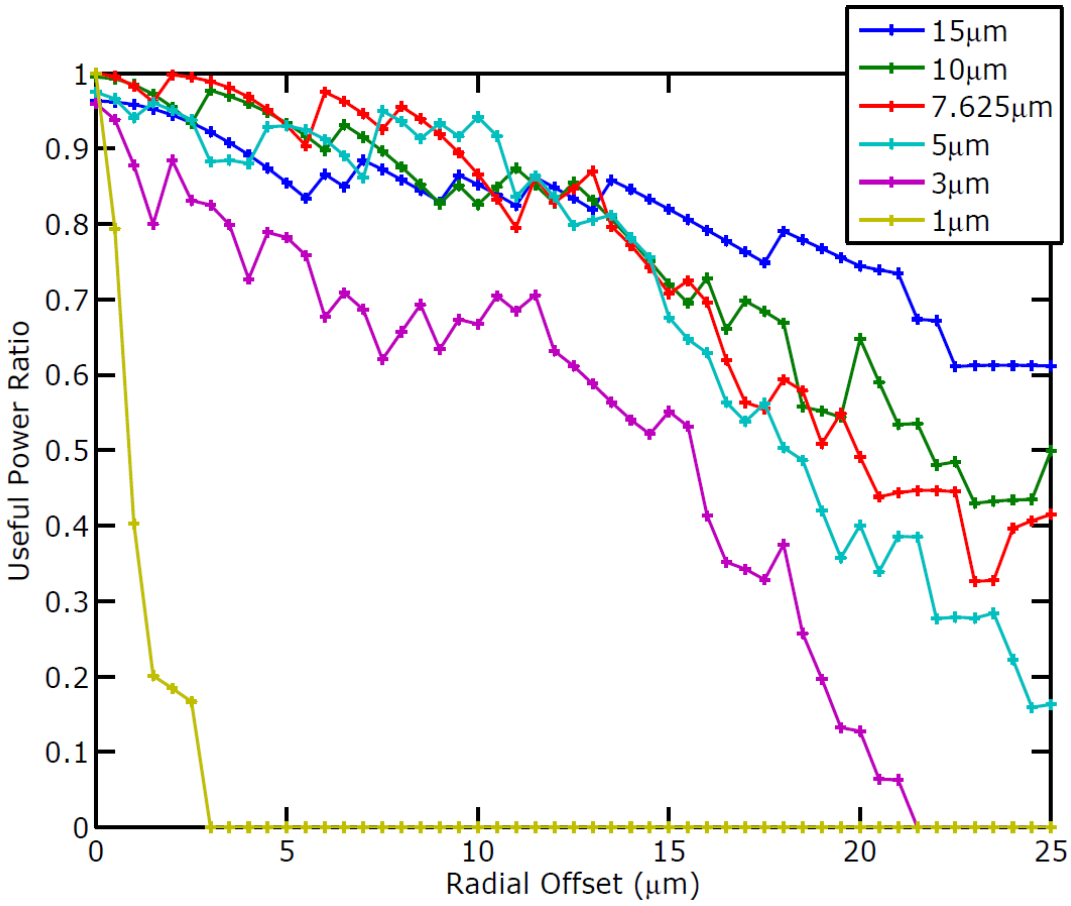

Figure 3.5: "Useful Power Ratio" of a p = 0, l = 0 laser for various laser sizes as a function of radial offset

coupling coefficient threshold are useful, how much of the total coupled power ends up in

these modes? To answer this question, we define a quantity that is essentially the "Useful Power Ratio". This power ratio is given as:

$$\text{"Useful Power Ratio"} = \frac{\sum P_{\text{guided modes over threshold}}}{\sum P_{\text{guided modes}}} \tag{3.6}$$

For the same parameters used in the previous plot and a useful efficiency threshold of 5%, Figure 3.5 shows the useful power ratio for various laser sizes.

It can be seen that for larger offsets, the larger laser sizes exhibit a larger useful power ratio. For example, at an offset of 20 μm, the 3 μm laser exhibits a useful power ratio of around 15%. For the same offset, the 5 μm laser shows a useful power ratio of approximately 40%. We would like this ratio to be as high as possible. This implies choosing an operating offset as close to zero as possible, or in effect, centering the laser with respect to the fiber. For larger offsets, this plot implies that a laser with a larger mode field size should be chosen.

3.3 Tradeoffs and Conclusion

Section 3.2 detailed an example analysis of a laser operating in the fundamental mode with a wavelength of 1550 nm. The goal was to excite the highest number of guided modes and couple into the fiber as much power as possible. What do the above plots tell us? The highest number of modes we saw was 27 in Figure 3.2 for an offset of around 20 μm with a laser size of 3 μm and 5 μm. However, by Figure 3.4, at an offset of 20 μm, the total power efficiency coupled into the 3 μm laser is just shy of 80%, and falls quickly thereafter. In fact, the overall trend suggests that as the radial offset increases, the number of modes excited increase, but the total power efficiency coupled into the fiber decreases. This presents a tradeoff between the two. Moreover, recall that the 27 modes excited all contain $\geq 1\%$ of

the input power, but, most of these modes $\leq 5\%$ of the input power which might not be enough depending on the channel; most of the modes contain little power. This can be seen by the useful power ratio plot in Figure 3.5 by the sharp decrease for the smaller laser sizes. Ultimately, the laser size and offset that should be selected depends on the channel and how much power is needed in each mode. If not much power is needed in each mode, it is best to select a relatively large offset and a smaller size laser. But, if significant power is required in each mode, it is best to select a larger laser size and a smaller offset.

Chapter 4

Systematic Calculation of Channel Capacities

The previous chapter described simulations to deduce the best parameters for one laser to be launched into multimode fiber with the aim of exciting the maximum number of modes upon launch. It was argued in Section 2.2 that launching into a large set of modes increases the likelihood of having independent, uncorrelated entries in the MIMO system matrix. This observation allowed an initial study to be performed (and trends to be deduced; see Section 3.3) while sparing the complexities associated with propagation in optical fibers. However, initial launch conditions alone cannot illuminate quantitatively the increased capacity benefits that MIMO affords. For quantitatively describing the benefits, we cannot shy away from complexity anymore, and are forced to tackle a propagation model for the channel and calculate the MIMO system matrix associated with it. Recall that the placement of the transmission and receive elements in the MIMO system is critically important, because placement affects the modes that are launched into the fiber. This chapter will bridge the gap, taking the guided modes that are launched, propagating them through the fiber from which the MIMO matrix $\mathbf{H}$ is derived. Since device placement is important, this chapter will describe the search for the optimal placement locations in a combinatorial fashion, which unfortunately, turns out to be a computational mess. Interestingly, the analogous problem of antenna placement in wireless MIMO systems has long been considered [11].

This chapter is divided into the following sections. Section 4.1 describes the power diffusion propagation model that we first considered and then talks about the matrix-based model that we actually implemented. It proceeds to describe the origin of intermodal coupling and how the model accounts for this coupling. Lastly, it introduces the statistical nature of the model. Section 4.2 highlights the simulation of channel capacities and how to actually calculate the capacity from the propagation model of the channel and device locations. Section 4.3 studies the optimal device placements by means of an exhaustive search and in the process gives proof that MIMO in optical MMF channels works. Section 4.4 discusses the tolerances of the optimal device placements when perturbed by either a lateral shift or rotation of the grid of devices. Lastly Section 4.5 summarizes the results of this important chapter.

4.1 Propagation Models

The capacity of a MIMO system depends on the diversity gain, in our case, the independent (orthogonal) spatial guided modes propagating in the fiber. In Chapter 3, we looked at the modes that are excited upon launch in trying to maximize diversity. In an ideal optical fiber, the distribution of modes upon launch will stay constant as the light propagates through the channel. However, no fiber is ideal, and the distribution of modes evolves within the fiber. As the modes propagate in the fiber, attenuation, or power loss can be experienced, along with power exchange between the modes, called intermodal coupling. The goal of this section is to capture and characterize mathematically intermodal coupling and the evolution of the distribution of modes.

4.1.1 Power Diffusion Model

The first model that we considered is called the power diffusion model. An early development of this model was considered by D. Gloge at Bell Labs [12]. To model the intermodal coupling, Gloge thought of the power present in each mode as a diffusion whereby power "leaks" into its nearest-neighbor modes. Gloge formulated a partial differential equation of two variables, the mode index taken as a continuous variable (better assumption with more modes present) and the propagation distance into the fiber. All one needs to do is solve the differential equation and evaluate it for the desired mode and distance. The power flow equation that Gloge developed is given by [12]:

$$\frac{\partial P}{\partial z} = -\alpha(\theta)P + (\Delta\theta)^2 \frac{1}{\theta}\frac{\partial}{\partial\theta}\left[\theta d(\theta)\frac{\partial P}{\partial\theta}\right] \tag{4.1}$$

In this equation, $P(\theta, z)$ is the function that we are trying to solve, where θ is the mode and z is the longitudinal distance into the fiber. More precisely, θ represents a group of modes with approximately the same transverse wave number (hence approximately the same angle) when dealing with cylindrical symmetry as in a multimode optical fiber. In light of this, the function P then gives the power in each mode in the mode group indexed by θ. Recall that different modes propagate in the fiber at different angles to the optical axis (See Section 2.1.3), hence the modes can be labeled by their angles. The function $\alpha(\theta)$ represents mode-dependent loss, and the function $d(\theta)$ represents the coupling strength of mode group θ to its nearest-neighbors. The first term in the equation gives the rate of change in z of power loss due to energy dissipation or attenuation. Note that it is proportional to the power in the mode itself. Now, Gloge uses the symmetry of the cylindrical fiber to deduce that α should be an even function and expands this function while keeping only the first two terms,

thus [12]:

$$\alpha(\theta) = \alpha_o + A\theta^2 \tag{4.2}$$

The solution can now be separated into $P(\theta, z) = \tilde{P}e^{-\alpha z}$ with the exponential part dividing out. Moreover, for the mode-specific coupling strength, Gloge assumes the constant $d(\theta) = d_o$. This implies that each mode group couples equally into its nearest-neighbor. With this in mind, Gloge derives his final diffusion-type differential equation in a continuous variable as [12]:

$$\frac{\partial P}{\partial z} = -\alpha(\theta)P + D\frac{1}{\theta}\frac{\partial}{\partial \theta}\left[\theta\frac{\partial P}{\partial \theta}\right] \tag{4.3}$$

The symbol D is actually a constant that includes in it the coupling strength d_o. Gloge then continues with the formulation and gives an experimental value for the constant $D = 7 * 10^{-5}\frac{\text{rad}^2}{\text{m}}$.

The main problem with the above formulation is that it assumes that the coupling strength is constant across mode groups. This seems like a relatively weak assumption. Other formulations of the diffusion-style coupling scheme have been developed and attempt to refine the coupling strength [13, 14]. While understanding the power distribution and its diffusion-style evolution is useful for the acquisition of quantities as the index profile of the fiber [14], they lack detail about how the perturbations in the optical fiber truly affect intermodal coupling. Moreover, a model based on a more dynamic electric field picture (rather than just powers) that accounts for polarization would be useful.

4.1.2 Matrix-Based Model

In light of the shortcoming of the diffusion-style propagation model, we choose a matrix-based model developed by M. B. Shemirani *et al.* [15]. This model is preferred

because it accounts for a detailed perturbative framework. Also, polarization-mode coupling is allowed and it is a matrix-based approach. The matrix relates the modes that are present upon incidence on the fiber to the modes that are present at the output; in essence it is a propagation matrix. The reason that a matrix-based approach is useful is because then this propagation matrix can be used in calculating the MIMO system matrix **H** (see Section 4.2).

To calculate the modes that are present at the input facet of the fiber, a light source is butt-coupled to the facet whose electric field profile is expanded by the fiber eigenmodes. To find the expansion coefficients in the expansion of the incoming electric field profile with the basis of fiber eigenmodes, we take the inner product of the incoming field and the eigenmodes. The expansion coefficients in this case are complex numbers whose magnitude squared represents the fraction of the power contained in the mode (assuming the eigenmodes are normalized), that is $\sum_{i,j} \left|\tilde{c}_{i,j}\right|^2 = \left|E_{input}\right|^2$, and the phase of the complex coefficients represents the initial phase given to the mode. Recall from Eq. 2.7 that the eigenmodes of the cylindrical fiber are the Gauss-Laguerre modes which exhibit circular symmetry on the transverse plane of the fiber. These form a basis for the expansion of incoming electric fields, but they are by no means the only basis. In fact, Shemirani uses the Hermite-Gauss modes (a basis in rectangular coordinates) instead since perturbations by the fiber will be easier to calculate in rectangular coordinates [15].

There comes the question of which set of modes is generally observed in real optical fibers. Mathematically, it does not matter in which basis the input electric field is expanded. Therefore, there exists a transformation between any two bases that can be found, and in fact was done so for the Hermite-Gauss and the Gauss-Laguerre bases in [16]. It was found that there does not seem to exist a mathematical equivalence between the two bases (though they

can both equivalently be used) and furthermore, that the Gauss-Laguerre modes are more "exotic" and hence even in real optical fibers with cylindrical geometry, nature preferred the rectangular Hermite-Gauss modes [16].

The Hermite-Gauss modes take the form [15]:

$$HG(x,y,z)_{p,q} = \frac{\sqrt{\frac{2}{\pi}}}{w\sqrt{2^{p+q}p!q!}} H_p(\sqrt{2}\frac{x}{w}) H_q(\sqrt{2}\frac{y}{w}) \exp(-\frac{x^2+y^2}{w^2}) \exp(-j\beta_{p,q}z) \tag{4.4}$$

The function given by H_p is to be interpreted as the p^{th} Hermite Polynomial. Let E_L be an incoming electric field vector and find each expansion coefficient $\tilde{c}_{p,q}$ by using Eq. 2.10. Keeping the Hermite-Gauss basis in mind, we form a vector whose entries are these complex coefficients. In vector form, the input electric field takes the form [17]:

$$\underline{a}_L = \begin{bmatrix} \langle E_L, E_{F_1} \rangle \\ \langle E_L, E_{F_1} \rangle \\ \vdots \\ \langle E_L, E_{F_M} \rangle \end{bmatrix} \tag{4.5}$$

where $\langle E_L, E_{F_j} \rangle$ represents the complex coefficient associated with the j^{th} fiber mode in the expansion of E_L. Note that the following vector is a $M \times 1$ vector where M represents the number of guided modes in the fiber. As an example, [17] mentions that for a fiber of 50 μm diameter, a referactive index of the core of 1.45, a core-cladding index difference of .001, and an operating wavelength of 1550 nm, the fiber includes 55 guided modes. Actually, because [15] considers coupling and distinguishes the two orthogonal states of polarization, there will actually be twice the number of propagating modes, 110.

Generally speaking, a MIMO system will consist of multiple lasers, hence, each laser will have an input vector associated with it. Grouping all these vectors as columns of a

matrix, we get our input light-field matrix $\mathbf{A}_L$ [17]:

$$\mathbf{A}_L = \begin{bmatrix} | & | & \cdots & | \\ \underline{a}_{L_1} & \underline{a}_{L_2} & \cdots & \underline{a}_{L_{N_L}} \\ | & | & \cdots & | \end{bmatrix} \tag{4.6}$$

The matrix $\mathbf{A}_L$ represents the laser matrix whereby each column i represents the input vector of the i^{th} laser. At the output facet, photodetectors are butt-coupled and act as a dual to the lasers at the input. Associated with each photodetector, there is a field pattern onto which the output light at the laser can be projected to find the excitation of the detector. The vector that represents this projection is given by $\underline{a}_D$ and placing all these vectors as columns of a matrix, we get the detector matrix $\mathbf{A}_D$ [17]:

$$\mathbf{A}_D = \begin{bmatrix} | & | & \cdots & | \\ \underline{a}_{D_1} & \underline{a}_{D_2} & \cdots & \underline{a}_{D_{N_D}} \\ | & | & \cdots & | \end{bmatrix} \tag{4.7}$$

To transform the input light-field matrix to the output facet of the fiber, we come up with the propagation matrix. A fiber is broken into N small sections whereby each section will have a section propagation matrix $\mathbf{U}_i$ such that $\mathbf{U}_{total} = \prod_{i=1}^{N} \mathbf{U}_i$ where the first fiber section corresponds to $\mathbf{U_1}$ and the output of the fiber is at the end of the $\mathbf{U}_N$ section [15]. The idea is to look at each small section and consider the perturbative effects of each. The section matrix is broken up into three different matrices, one for each of three physical transformations. First, we consider a propagation matrix that includes information on the coupling from each mode to another, mode-dependent loss, and a phase accumulation term for the particular fiber section at hand; such matrix will be labeled $\mathbf{U}^i_{prop}$ [15]. The transformation given in this matrix can be seen visually in Figure 4.1.

A second matrix, $\mathbf{R}^i$, accounts for the polarization changes that occur in the fiber due to twisting of the fiber. Since it only changes the polarization direction, it is a unitary

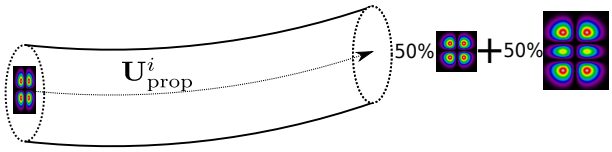

Figure 4.1: $\mathbf{U}^i_{\text{prop}}$ is a random matrix that describes intermodal coupling with in a section. In particular, it transforms a vector containing the weights of each guided mode to provide a vector which has the new weights after the signal has undergone intermodal coupling within the fiber section.

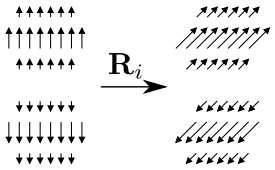

Figure 4.2: $\mathbf{R}^i$ is a random matrix that describes rotation of the polarization of the electric field at section junctions. It rotates the polarization of each mode within the fiber section based upon propagation effects of the fiber.

matrix that is given by the expression [15]:

$$\mathbf{R}^i = \begin{bmatrix} \cos(\theta_i)\mathbf{I}_{M\times M} & \sin(\theta_i)\mathbf{I}_{M\times M} \\ -\sin(\theta_i)\mathbf{I}_{M\times M} & \cos(\theta_i)\mathbf{I}_{M\times M} \end{bmatrix} \tag{4.8}$$

The reason the identity matrix $I_{M\times M}$ is in this expression is because the x and y components of the electric field vectors are actually vectors themselves representing the component in the Hermite-Gauss basis. Each representation must rotate, that is, the representation vector for the x and y polarization. Pictorially, this transformation is given in Figure 4.2

The third matrix, $\mathbf{M}^i$ represents a rotation of the mode field pattern in whole and is also due to the twisting of the fiber at the section interfaces [15]. It can be seen in Figure 4.3.

The effect of these three matrices is then combined to give the section matrix as $\mathbf{U}_i = \mathbf{M}^i\mathbf{R}^i\mathbf{U}^i_{prop}$ [15]. Then, the total transformation matrix of the fiber is given by $\mathbf{U}_{total} = \prod_{i=1}^{N} \mathbf{U}_i$. Figure 4.4 shows the input and output electric field profiles for some 2×2 and

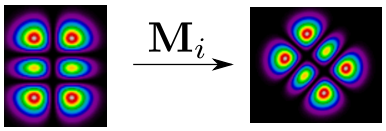

Figure 4.3: $\mathbf{M}^i$ is a random matrix that describes rotations of the electric field profile due to fiber twists within the i-th fiber section.

3×3 MIMO system (first number corresponds to number of lasers and second to number of detectors). The input profile is calculated from combining the fundamental modes of the lasers and the outputs show the respective light pattern after propagation through the fiber by application of $\mathbf{U}_{\text{total}}$.

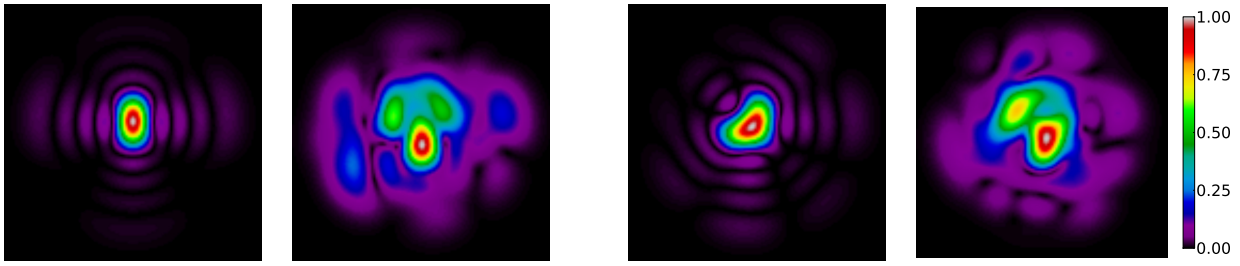

(a) (b) (c) (d)

Figure 4.4: Calculated normalized electric field patterns at the fiber input and output facets: (a) 2×2 input field profile, (b) 2×2 output field profile, (c) 3×3 input field profile, (d) 3×3 output field profile.

4.1.2.1 Origin of Intermodal Coupling

It is illuminating to consider how the $\mathbf{U}^i_{prop}$ matrix is derived. In it, is contained information about how the different modes mix with each other in propagation along the length of the fiber. Deriving the matrix elements requires a model for the energy exchange between modes. Shemirani attributes this exchange process to the bending of the fiber section. When the fiber is bent along sections of the fiber, the index of refraction profile

changes from its perfect cylindrical structure. In what follows, we consider a perturbative analysis of the index of refraction following the work of Shemirani [15]. Assuming the fiber is perfectly centered about the z-axis, the graded index of refraction (parabolic) takes the form:

$$n^2 = n_o^2 - 2\Delta n_0^2(\frac{\sqrt{x^2+y^2}}{a})^2 \tag{4.9}$$

where a is the core radius of the fiber and n_o is the core index. If the fiber is bent and without loss of generality, we assume that the bending occurs in the x-direction such that at position z the center of the fiber is at $(x_o(z), 0)$, then the new index of refraction profile can be written as:

$$n^2 = n_o^2 - \frac{2\Delta n_o^2}{a^2}((x - x_o(z))^2 + y^2) \tag{4.10}$$

Now, we expand $((x - x_o(z))^2 + y^2) = x^2 - 2xx_o + x_o^2 + y^2$, and neglect the x_o^2 term because we are assuming small deviations of x_o. Notice that:

$$n^2 = n_o^2 - \frac{2\Delta n_o^2}{a^2}x^2 - \frac{2\Delta n_o^2}{a^2}y^2 - \frac{2\Delta n_o^2}{a^2}2xx_o = n_o^2(1 - \frac{2\Delta}{a^2}x^2 - \frac{2\Delta}{a^2}y^2 - \frac{2\Delta}{a^2}2xx_o) \tag{4.11}$$

The first three terms of Eq. 4.11 represent the actual unperturbed index of refraction while the fourth term represents the perturbative correction. For this to be a valid perturbative analysis, $\frac{2\Delta}{a^2}2xx_o \ll 1$.

Shemirani shows that the coupling coefficient between mode p, q and p', q' is given by:

$$C_{pq,p'q'} = \frac{k_o}{2n_o}\left\langle E_{pq}\left|\frac{\frac{\partial n^2}{\partial z}}{\beta_{pq}-\beta_{p'q'}}\right|E_{p'q'}\right\rangle \tag{4.12}$$

It can be seen from this equation that the cause of coupling between the modes is in fact the perturbative bending of the fiber section. Note that the bra-ket factor relies on there being a change in index of refraction along the propagation direction that is non-zero (for

different modes). In an ideal fiber, there exists translational invariance along the z-direction, but when bends are present there will be an index of refraction change and the stronger this change, the stronger the breakage of symmetry and a potential for coupling. The expression in Eq. 4.11 is plugged into Eq. 4.12 and accounting for a change of the x-axis due to bending, results in:

$$C_{pq,p'q'} = j\frac{2k_o n_o \Delta}{a^2}\frac{\frac{dx_o^2(z)}{dz^2}}{(\beta_{pq} - \beta_{p'q'})^2}\left\langle E_{pq}\left|x\right|E_{p'q'}\right\rangle \tag{4.13}$$

Shemirani models the fiber bends by specifying that the center of each fiber section has an x-coordinate of:

$$x_o(z) = \frac{1}{\kappa}(1 - cos(\kappa z)) \approx \frac{1}{2}\kappa z^2 \tag{4.14}$$

In this equation, κ is the radius of curvature of the sectional bend where the latter approximation becomes more accurate when the sections of the fiber are shorter. According to Eq. 4.13, the second derivate of $x_o(z)$ is taken and all there is left to evaluate is the matrix element with the x-coordinate operator that causes overlap between different modes. Using the functional expression for the electric field, selection rules can be readily obtained and it is seen that the matrix element takes a non-zero value only for nearest-neighbor modes in the p mode number with equal q mode number.

The coupling coefficient expression is then used in a differential equation in the longitudinal direction that gives the evolution of the amplitude of a mode as it propagates in a section and is used in a modal-loss term in the differential equation. Since each mode has its own differential equation, we have a set of differential equations that can be cast in matrix form, and using the matrix exponential, can be solved to give the sectional propagation matrix that we seek.

4.1.2.2 Statistical Nature of Fiber Model

A communication channel is statistical by nature and fluctuates in time, thus signals through the channel will experience different transformations when launched at different times. The capacity through a channel must be calculated as an average of the maximum data rate over (theoretically) all channel realizations. A channel realization is a particular physical state that the channel takes with a particular transmission characteristic. The more realizations that are available, the better the averaging process becomes which leads to a more accurate calculation of the capacity. In the matrix model that is described in Section 4.1.2, a particular realization of the channel translates to knowing the propagation matrix for the channel, $\mathbf{U}_{total}$. How does the matrix model allow for different channel realizations, that is, what in the model allows for different propagation matrices representing the realizations? The answer lies in the introduction of random variables in the model. In particular, the radius of curvature κ_{i} of the i^{th} fiber section is a random variable, and the angle θ_{i} that represents the rotation of the i^{th} fiber section with respect to the $(i+1)^{\mathrm{th}}$ section is also a random variable [15]. Both of these variables are modeled as i.i.d normal distributions. κ enters the model as seen in Eq. 4.14 which affects the sectional propagation matrix $\mathbf{U}_{\mathrm{i}}$, and θ enters in the $\mathbf{R}^{\mathrm{i}}$ as seen in Eq. 4.8 and $\mathbf{M}^{\mathrm{i}}$ matrix.

4.2 Generating Channel Realizations

Now that we are equipped with a propagation model, we are ready to simulate the capacity for various MIMO systems. Given a particular channel realization, the next thing that must be done is to choose the placement of lasers and detectors at the end facets of the fiber. Reiterating, placement of these devices affect the number of modes that are excited

in the fiber and we speculated that this will ultimately affect the capacity of the channel due to the diversity gain. Each different placement configuration leads to a different MIMO system matrix. In this section, we describe how to calculate the MIMO system matrix, how to calculate the capacity associated with the matrix, and discuss a simulation of different placement configurations and give device placement strategies.

The MIMO system matrix can be calculated by applying the propagation matrix on the input laser matrix and then projecting that result onto the detector matrix as [17]:

$$\mathbf{H}(t) = \mathbf{A}_D^H \mathbf{U}_{\text{total}}(t) \mathbf{A}_L \tag{4.15}$$

Once we have the system MIMO matrix, the capacity of the channel is the metric we are interested in maximizing, and it can be evaluated using the formula [18]:

$$C = \mathbb{E}\left(\log\det\left[\mathbf{I} + \frac{1}{N_L}\mathbf{H}\mathbf{H}^{\star}\right]\right) \text{ bits/s/Hz} \tag{4.16}$$

The maximization of the capacity is performed over the space of possible laser and detector configurations. To simplify the simulation, a $N \times N$ grid of possible device placements is centered about each end facet of the fiber. Each point on this grid represents a possible device location. This implies that if all the grid points contained actual devices, we would have a $N \times N$ MIMO system with N lasers and N detectors. If the number of devices is smaller, there are multiple combinations of device placement positions that can be considered and whose capacity must be compared. For a $N_L \times N_D$ MIMO system where N_L is the number of lasers used and N_D is the number of detectors used, the number of comparisons is $\binom{N^2}{N_L} \times \binom{N^2}{N_D}$. In this chapter, we consider an exhaustive search for the best configuration that yields the maximum capacity whereby all of the combinations will be compared and

the best chosen. While this technique certainly yields the configuration that maximizes the capacity, the problem is that if the possible grid of device locations is large, that is, the grid is fine, then the number of comparisons for the optimal configurations can become prohibitively large. For example, for a 5×5 grid and a 10×10 MIMO system, we have $\binom{25}{10} \times \binom{25}{10} \approx 10^{13}$ comparisons to make. This exhaustive technique becomes prohibitive very quickly. Nonetheless, for coarse grids, it can provide the guaranteed maximal capacity, and is useful in demonstrating that capacity gains are indeed afforded by optical MIMO. Moreover, the exhaustive technique shows that device configurations indeed affect the capacity, hence implying that a best configuration should be sought.

The simulation is performed in MATLAB to determine the device configuration that yields the maximal capacity over an ensemble of channel realizations. It should be noted that an ensemble of system realizations translates to an ensemble of $\mathbf{U}_{\text{total}}$ matrices, and therefore, an ensemble of MIMO system matrices $\mathbf{H}$ that can then be averaged to find the capacity. In our simulations, an ensemble means generating 700 $\mathbf{U}_{\text{total}}$ matrices that are broken into $10,000$ sections each. Each section is taken to be 10 cm in length. The graded index fiber has a 50 μm diameter, a core index of refraction of 1.444, and a numerical aperture given by .19. The laser is taken to emit at a wavelength of 1550 nm which is a known low-loss window for glass fibers. The detectors are assumed to behave similarly to the lasers in terms of their light detection as an overlap between the modes of the fiber and the electric field profile of the photodetectors. Recalling the statistical nature of the fiber propagation model described in Section 4.1.2, the radius of curvature κ_i of each fiber section is a normal i.i.d random variable, and in this simulation, we take it to have a standard deviation of $\sigma^2_{\kappa_i} = .95$ m^{-1} , and the twisting angle between each section θ_i is taken to have a standard deviation

of $\sigma^2_{\theta_i} = .6$ radians as suggested by [15].

4.3 Device Placement Study

This section shows that optical MIMO is feasible by comparing a 1×1, 2×2, and a 3×3 MIMO systems resulting in an increase of capacity with an increasing number of devices. Secondly, once a particular number of lasers and detectors has been set, the particular configuration of these devices on the grids affects capacity, thereby implying there exists a best configuration, and these best placements are found for a 2×2 and a 3×3 MIMO system using the exhaustive search. We published the results of this section in [17].

4.3.1 Benefits of MIMO Using Exhaustive Search

A 3×3 grid is placed on the end facets of the fiber. A laser with mode field diameter of 12 μm is used. If N_L number of lasers is used and N_D number of detectors are used, then the number of possible configurations is $\binom{9}{N_L} \times \binom{9}{N_D}$. For each of the possible configurations (exhaustive search), the capacity is calculated using Eq. 4.16 over the 700 channel realizations, and the best configuration is chosen. Using this technique, we compare the maximum capacities of the 1×1, 2×2, and 3×3 MIMO systems. For the 1×1 system, the highest capacity is where the laser and detector are centered thus no comparisons are needed at all. Figure 4.5 shows the maximal capacity as a function of Signal to Noise Ratio (SNR). The figure shows that when the 2×2 and 3×3 MIMO systems are compared to the 1×1 MIMO system, at an SNR of 10dB, there is a gain of capacity of approximately 50% and 80% respectively. This result proves that optical MIMO is feasible and affords significant gains in capacity.

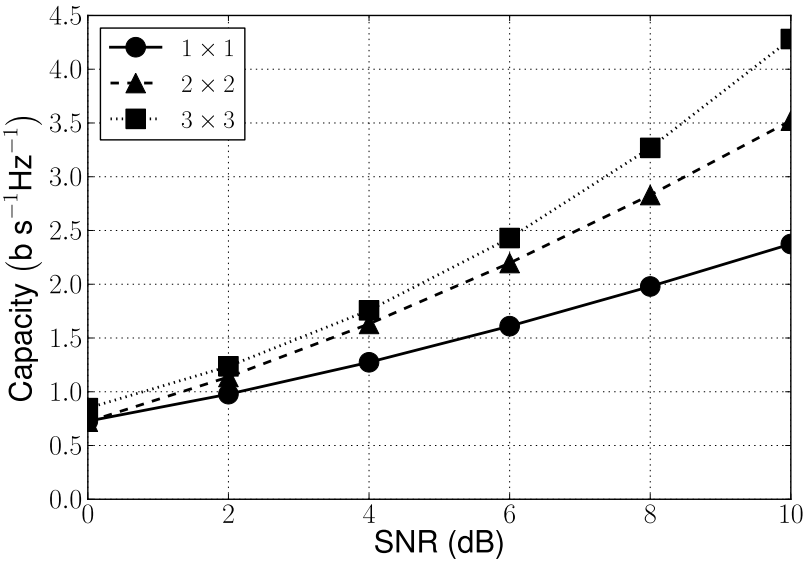

Figure 4.5: Capacity vs. SNR for 1×1, 2×2, and 3×3 MIMO systems for the best device configuration

4.3.2 Selection of Optimal Device Configuration Using Exhaustive Search

To show that the selection of device placements affects capacity in a MIMO system, we compare the capacity of two configurations, one suboptimal configuration and the optimal configuration for a 2×2 and a 3×3 MIMO system. The same grid and device sizes are used as in Section 4.3.1.

Figure 4.6 compares the Capacity vs. SNR for the two configurations of a 2×2 MIMO system. It can be seen that at an SNR of 10dB, by selecting the best device configuration, the capacity is increased about 1.75 times that of a suboptimal one. Figure 4.6(a) shows the laser and detector configurations that yield the maximal capacity and Figure 4.6(b) shows the laser and detector configurations of a representative suboptimal configuration.

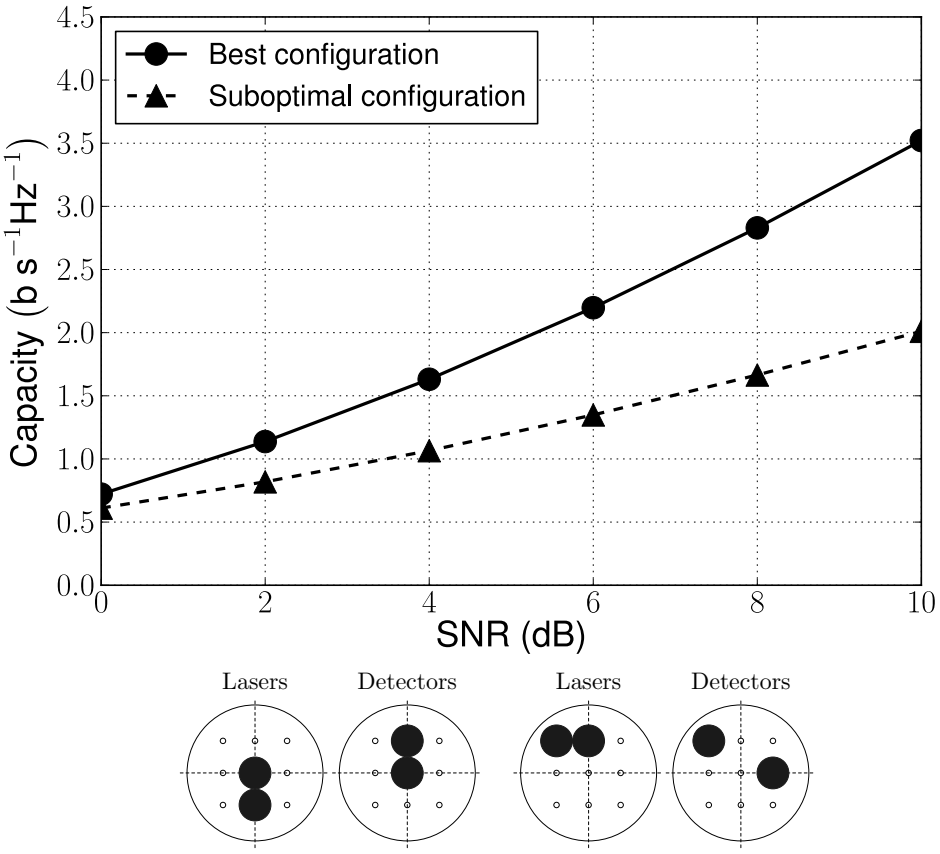

(a) Best Configuration (b) Suboptimal Configuration

Figure 4.6: Capacity vs. SNR for a 2×2 MIMO system for the best device configuration and a suboptimal configuration in the plot above. The four circles at the bottom represent the fiber cross sections and the laser and detector placements on the cross sections that yielded both the best and suboptimal configurations. The small open white circles represent the grid points of allowed device positions and the large black circles represent the specific device placements associated with the configurations.

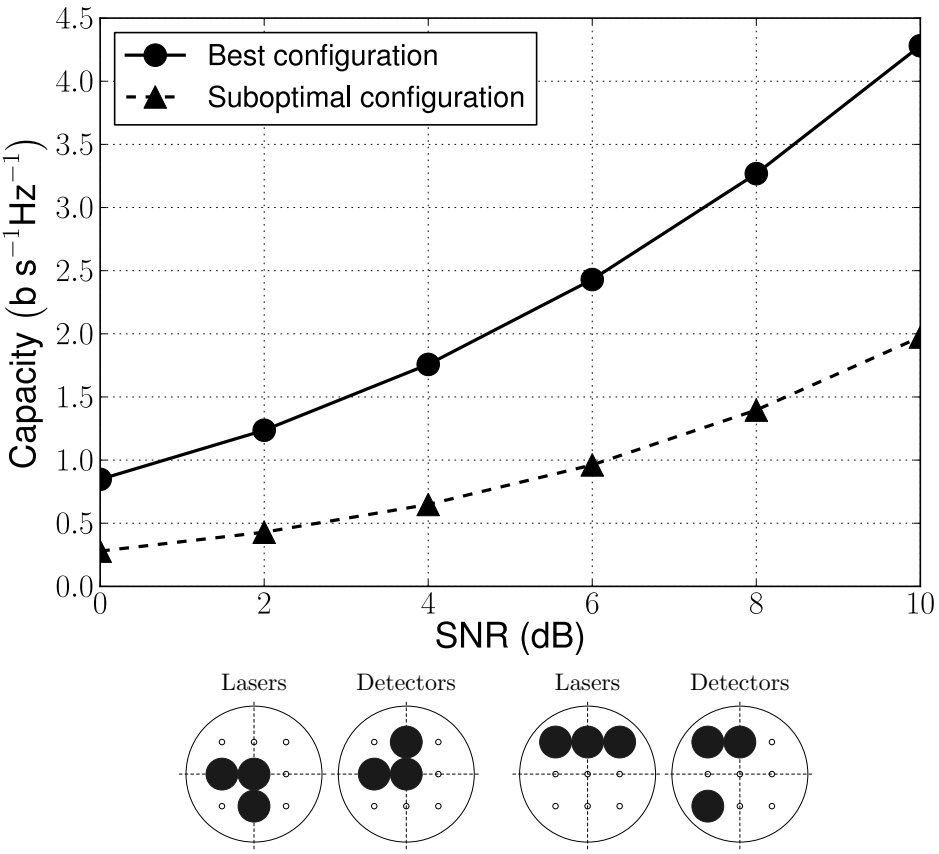

(a) Best Configuration (b) Suboptimal Configuration

Figure 4.7: Capacity vs. SNR for a 3×3 MIMO system for the best device configuration and a suboptimal configuration in the plot above. The description of the sub figures is similar to that in Figure 4.6.

A similar analysis is performed for a 3×3 MIMO system as can be seen from Figure 4.7. At an SNR of 10dB, the optimal configuration yields over twice the capacity of the representative suboptimal configuration. For the 3×3 MIMO system, Figure 4.7(a) shows the laser and detector configurations that yield the maximal capacity and Figure 4.7(b) shows the laser and detector configurations of a representative suboptimal configuration.

From these plots, it is seen that the central point of the device grid activates the fundamental mode of the fiber which is prominent in propagation at large distances through the fiber and hence the optimal configuration will utilize this central position. Moreover, selecting the optimal device placement is crucial to the maximization of the capacity.

4.4 Device Placement Tolerances

In the previous section we showed that it is critically important to select the optimal device configuration to maximize the capacity of our system. However, the grid positions that were suggested assumed that the grid was perfectly centered about the fiber. A good way to visualize it is as a square inscribed in a circle. What happens to the capacities if the grid or square is rotated by some angle whereby the devices placed on the grid, those found from the optimal configuration are now rotated? What happens to the capacities if a lateral shift is made? These perturbations from the centered grid provide a realistic scenario whereby a real grid might not be placed perfectly about the center. It is thus instructive to study the tolerance of the optimal configuration to the effect of perturbations of the grid.

Using the same parameters for the fiber as described in Section 4.2, and 12 μm diameter lasers and photodetectors, the best device configurations that maximize the capacity for a 3×3 grid are those given in Figures 4.6 and 4.7 for the 2×2 and 3×3 MIMO system

respectively. The grids for both of these configurations are shifted with respect to the fiber in the direction that yields the worst-case reduction in capacity. We offset the grids from the central aligned position to an offset of 5 μm in the worst-case direction and record the resulting capacity. Figure 4.8 shows the results of this offset. It can be seen by the figure that

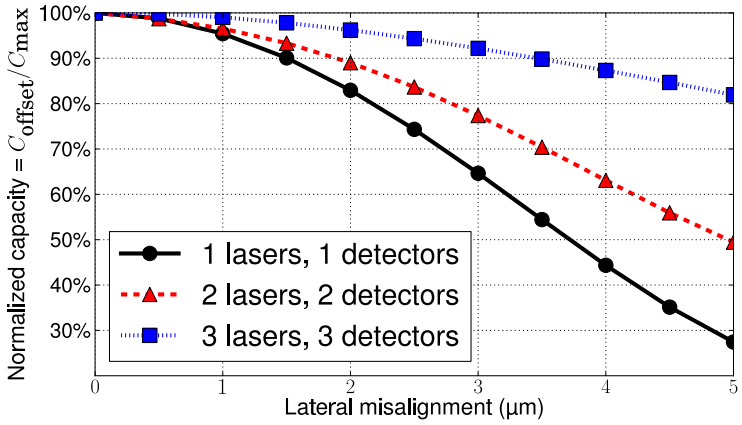

Figure 4.8: Calculated reduction of data rate capacity due to offset coupling for the 2×2 and 3×3 cases relative to the maximum obtainable data rate for lateral misalignments

the larger the number of devices, the more tolerant the optimal configuration is to lateral shifts. In fact, the 3×3 MIMO system only drops to 80% of its maximal capacity when shifted by 5 μm. We believe that the reason that a higher number of devices leads to more tolerant configurations is because the effective coupling area is higher, and hence a small lateral shift reduces the overlap a smaller fraction than if a small coupling area exists, as in the 1×1 MIMO system.

The second tolerance study that is performed is an angular rotation of the grid with respect to the perfectly aligned optimal configuration through 360°. Figure 4.9 shows the fraction of the optimal capacity that is achieved as a function of grid rotation angle both for

the optimal 2×2 and 3×3 MIMO system. It can be seen from the figure that for both of

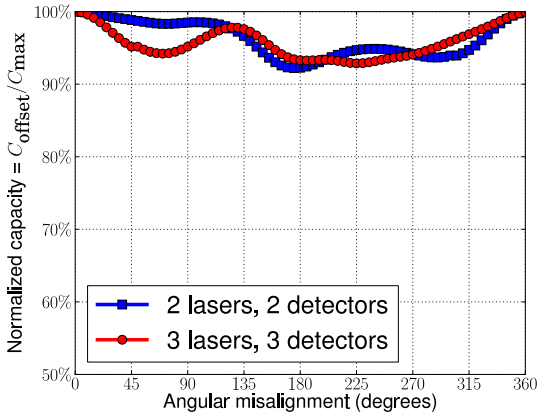

Figure 4.9: Calculated reduction of data rate capacity due to offset coupling for the 2×2 and 3×3 cases relative to the maximum obtainable data rate for angular misalignments.

the systems, there is a strong tolerance to rotations, as can be seen from the fact that the fraction of the optimal capacity achieved never drops below 90%. We speculate that this is due to the fact that due to intermodal coupling in the fiber, a distance of 1 km is long enough to spread the energy over a range of modes that is relatively independent of rotation angle. Note that rotations don't change the overlap between the incoming light pattern and the fiber eigenmodes in the same drastic way as lateral offsets, which is why we see better tolerances for rotations than for offsets.

4.5 Summary

In this chapter, a systematic calculation of the capacities of various MIMO systems was performed. To calculate the capacities, an ensemble of channel realizations was needed. For channel realizations, a statistical propagation model needs to be considered. A diffusion-

style propagation model was discussed, but was found to be lacking in detail of intermodal coupling. A better model was found to be the matrix-based model developed by Shemirani that accounts for intermodal coupling by considering fiber index of refraction perturbations [15]. Using this model, we generated an ensemble of channel realizations and found the MIMO system matrix for a particular realization by considering the laser and photodetector configurations. Then, we established the ergodic capacity to be the metric we would like to maximize. With this metric, we simulated a 1×1, 2×2, and 3×3 MIMO systems and found that as the number of devices increase, so does the capacity through the channel proving that optimal MIMO is feasible. Moreover, we saw that device placement on the input and output facets are important and found the optimal configurations for our simulated MIMO systems. The last section considered the tolerances of the optimal configurations to perturbations in the form of lateral grid offsets and grid rotations and we found that as the number of devices increase, so does its tolerance to the perturbations.

Chapter 5

Greedy Device Placement Algorithm

In the previous chapter, we used an exhaustive search to maximize the capacity of a given $N_L \times N_D$ MIMO system by comparing all possible device placement configurations and choosing the one that maximizes the capacity. While this method is guaranteed to yield the optimal device configuration, the exhaustive search becomes computationally burdensome when a large search-space is present, that is, a fine grid with many possible placement points. To alleviate the search complexity (search time), we note that when the configuration of lasers is fixed, the ergodic capacity is submodular in the selection of detector placements [19]. This lends itself to a greedy algorithm of detector placement selection whereby the detectors are placed on the grid sequentially, each detector being placed at the position that will maximally increase the capacity given the placement of the previous detectors. To see the benefits of such a selection algorithm, consider a 2×2 MIMO system placed on a 4×4 grid. Fixing the position of the lasers, the number of comparisons required for the exhaustive search is $\binom{16}{2} = 120$ whereby a greedy selection algorithm would require only $16 + 15 = 31$ comparisons. The greedy technique clearly allows us to find a good device configuration with a minimal number of comparisons versus the exhaustive technique, but, at a cost. We know that the exhaustive technique is guaranteed to yield the optimal device configuration with the true "global" maximum for the capacity. The question becomes: Does the device configuration yielded by the greedy selection give us the highest capacity? If not, what

fraction of this maximum capacity can we hope to achieve? The answer to the first question is no, for it takes an exhaustive number of comparisons to *guarantee* the maximum capacity. Any algorithm with less comparisons must be suboptimal without any other information. As we shall see in the following Section 5.1, a fraction, or lower bound, of the true maximum can be guaranteed where any particular implementation can yield at least this lower bound, but often close to the true maximum. In Section 5.2, we show a simulation in which the greedy capacity is close to the maximal capacity. The results in this chapter are currently in preparation for publication at the time this thesis was written [19].

5.1 Submodularity Property

The computational benefits that are gained by using a greedy algorithm are enabled by what is termed the submodularity property. By showing that a particular function obeys submodularity over a set, a greedy algorithm can be used to optimize the function over certain subsets. In particular, taking a subset of detectors $S \subset D$ where $D = D_1, D_2, D_3, ..., D_{N_D}$ and D_i is the i^{th} detector, Theorem 1 of [19] proves that the capacity of S given by:

$$C_S = \log\det\left(\mathbf{I}_{|S|} + \frac{P}{N_D}\mathbf{H}_S\mathbf{H}_S^\dagger\right) \tag{5.1}$$

is submodular in the detector subsets. Moreover, it shows that the capacity is monotonically increasing whereby an addition of another detector to the set S will increase the capacity. With this theorem, and the guarantee that successive additions of detectors will increase the capacity, we can use a greedy selection algorithm to determine the optimal device configurations. The submodularity of this capacity can be extended to ergodic capacity, that is, over the ensemble of system realizations. Moreover, by Theorem 2 of [19], we see that the

greedy selection algorithm guarantees a capacity greater than a factor of $(1 - e^{-1})$ of the maximal capacity. In other words, if C_o is the optimal capacity that an exhaustive greedy search yields, and C_g is the capacity that a greedy search yields, then:

$$C_g \geq C_o(1 - e^{-1}) \tag{5.2}$$

What this tells us, is that while we cannot guarantee an optimal configuration that yields maximal capacity, we can at least guarantee a reasonable performance at a fraction of the computational cost. While this may seem like a limitation, for grid structures that are fine with many grid locations, an exhaustive search is all but impossible computationally, whereby the greedy selection at least provides us some solution.

5.2 Comparison of Exhaustive and Submodular Search

This section demonstrates the usefulness of the greedy selection algorithm by comparing the technique to the exhaustive one for a coarse grid and showing that the greedy search performs near optimally. Moreover, this section will explore the capacity for a fine grid with the use of the greedy search, and for which the exhaustive search is not possible.

5.2.1 Comparison of Exhaustive and Greedy Selection Algorithms

To facilitate comparison between the exhaustive and greedy algorithms, a grid that is coarse enough needs to be chosen such that the exhaustive search is computationally feasible. A 4×4 grid can be used for this task, and we consider a 2×2 MIMO system. As mentioned at the beginning of this chapter, the exhaustive search requires 120 comparisons whereas the greedy search only requires 31 comparisons. Figure 5.1 shows the capacity versus SNR

for both the exhaustive and greedy placement algorithms where the lasers are fixed as in Figure 5.1(a) and 5.1(b). These figures also show the detector configuration that is selected in optimizing the capacity by each of the two algorithms.

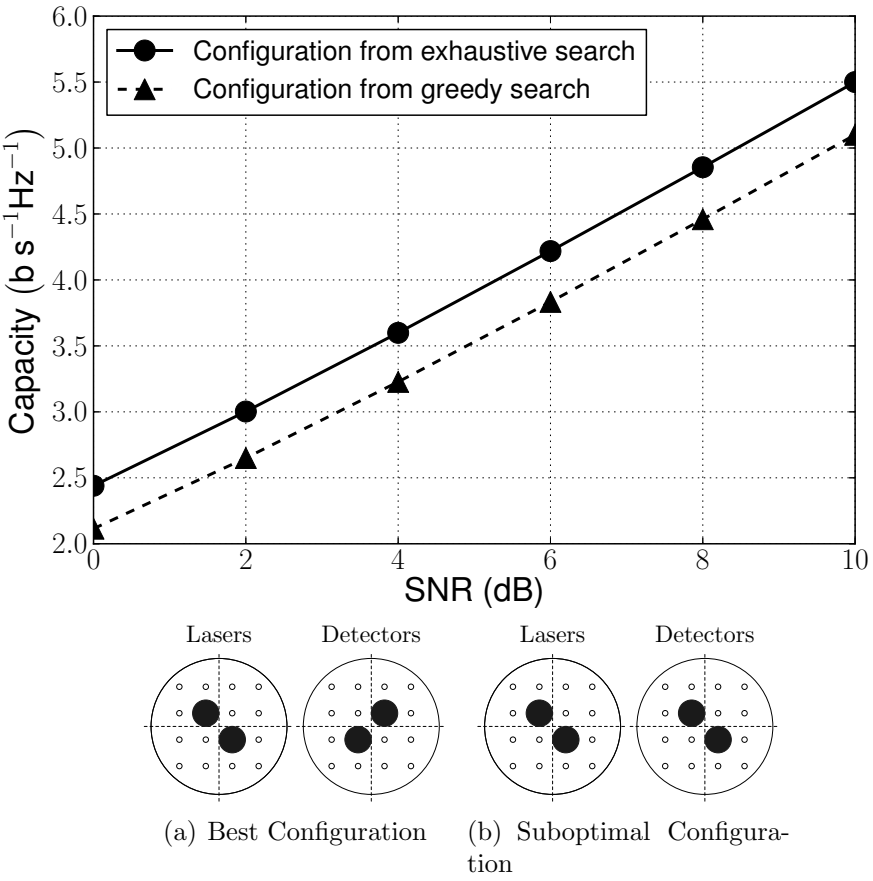

(a) Best Configuration (b) Suboptimal Configuration

Figure 5.1: Comparing the configurations obtained by the exhaustive search and the greedy search. It can be observed that about 92% of the capacity of the optimal exhaustive search can be obtained by the greedy search in this case.

It can be seen from the plot that at an SNR of 10dB, the greedy search achieves around 92% of the maximal capacity as calculated by the exhaustive search. This perfor-

mance for the greedy selection is achieved in only about 25% of the comparisons. It is well above the $(1 - e^{-1})$ lower-bound guaranteed by the theorem discussed in Section 5.1. This shows that particular MIMO implementations whose device configurations are found by a greedy algorithm can yield high capacities close to the optimal with a significantly reduced computational complexity. This example illustrates the feasibility of the greedy technique in providing an alternative, computationally friendly device placement algorithm.

5.2.2 Greedy Selection Algorithm for Fine Grids

For fine grids, the exhaustive selection technique is not feasible. We consider a 7×7, 9×9, and a 11×11 grid. For a 6×6 MIMO system, with the laser configuration fixed, an exhaustive search would require on the order of $\binom{49}{6} \approx 10^7$, $\binom{81}{6} \approx 10^8$, and $\binom{121}{6} \approx 10^9$ comparisons for each of the grids respectively. These are huge number of comparisons to make and thus render the exhaustive technique infeasible. Instead, we consider the greedy technique and calculate the capacity for each of these three grids. The fiber takes the size of 50 μm in diameter, and the lasers that are used are 5 μm in diameter. The lasers are fixed as in Figure 5.2.

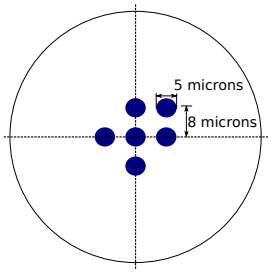

Figure 5.2: The laser array utilized with the 50 μm fiber. The lasers have a mode field diameter of 5 μm and a pitch of 8 μm

The greedy algorithm is used to select the best detector placements where the size of the detectors is taken to be 4 μm in diameter. These placement locations are shown in Figure 5.3.

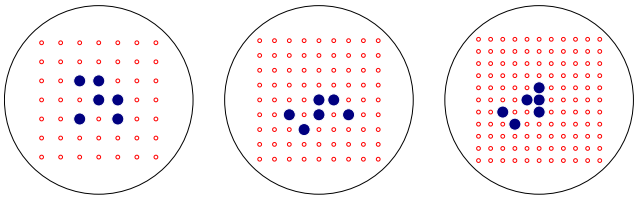

(a) 7×7 grid (b) 9×9 grid (c) 11×11 grid

Figure 5.3: The detector configurations obtained by the greedy algorithm for detectors of diameter 4 μm for various grid structures

The capacities associated with these placements are shown in Figure 5.4. The capacity plot shows that the capacity is improved from the 7×7 to the 9×9 grid, especially for higher SNR values, but the difference in capacity between the 9×9 and the 11×11 grid is not significant. This plot shows diminishing returns as the grid becomes finer. This is due to the fact that the capacity is strongly affected by how much overlap exists between the lasers and the fiber modes. As the grid becomes finer, the possible device positions are not significantly far in physical distance in relation to their neighbor positions hence not affecting the resulting overlap significantly and thus yielding a diminishing returns trend in the ensuing data rates.

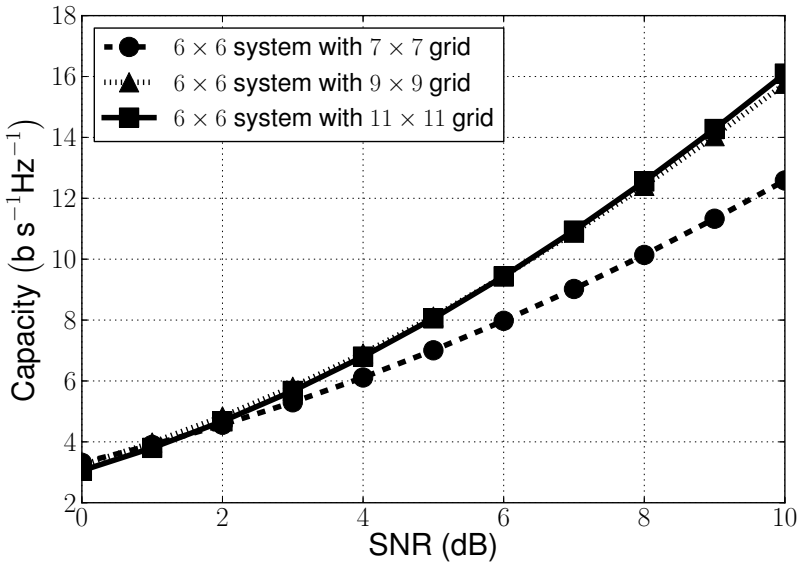

Figure 5.4: The capacity trends obtained with the detector configurations shown in Figure 5.3.

Chapter 6

Conclusion

This thesis shows through simulations the capacity benefits that are afforded by employing MIMO techniques to MMFs. The key idea rests on the multiple independent spatial paths present in the multimode fiber that leads to spatial gain that is shown in MIMO theory to increase capacities through wireless channels. Increasing the number of modes launched into the fiber increases the likelihood of having good properties to the MIMO system matrix. This realization led to studying the launch conditions that maximize the number of modes excited during input coupling of a single VCSEL to a MMF, a quick study that highlights the desirable launch conditions likely to increase capacity without the complexity of a full-blown propagation model. From this initial investigation, qualitative results show that as the number of modes launched that contribute to the diversity increases, the total power coupled into the fiber decreases, thus presenting a tradeoff. It is beneficial to increase the power through the channel to increase the SNR, but this leads to less modes being launched. To truly quantify the effects of MIMO, a propagation model was considered that yielded the MIMO system matrix for a particular channel realization. Effects such as intermodal coupling and mode rotation were considered. An ensemble of channel realizations was used to compare the ergodic capacity of a 1×1, 2×2, and 3×3 MIMO systems. It was seen that the 2×2 and 3×3 systems yield approximately a 50% and 80% increase in capacity respectively over the 1×1 system. Such result proves that MIMO is indeed useful

and clearly demonstrates the significant gains that can be had. Moreover, it was seen that the capacity of a particular MIMO system is a function of device placements on a grid placed at the input and output, therefore, there exists a best device geometry that must be sought, in this case, exhaustively. If these device grids are to be physically implemented, then it is imperative to study the effects of perturbations of the optimal device geometry from the perfect grid locations. Two effects were considered, a lateral offset of the whole device grid, and a rotation of the grid by some angle. The tolerance to lateral offset is stronger for a system with a larger number of devices, in particular, for a 5 μm lateral offset, the capacity of the 3×3 system diminished to 80% of its optimal capacity, while the 1×1 system reduced to less than 30% of its optimal capacity. On the other hand, the tolerance to rotations is good for both the 2×2 and 3×3 systems, staying above 90% of the optimal capacity as the grid was rotated through 360°. If the grid becomes finer, with more potential device placements, then the exhaustive search, though guaranteed to yield the optimal device configuration, becomes computationally cumbersome. It is noted that the when the laser grid is fixed, the selection of the optimal device configuration is submodular. This allows a greedy algorithm to alleviate the computational complexity of the exhaustive approach, but, at the price of only guaranteeing the resulting device geometry is greater than a $1 - e^{-1}$ fraction of the optimal geometry that would be found if an exhaustive search is performed. A comparison of the exhaustive and greedy search algorithm is performed for coarse grids and shows that in such case, the greedy search yields a device configuration with a capacity that is 92% of the optimal one found by the exhaustive search, yet requires only 25% of the comparisons. The greedy search is then used on fine grids to predict the capacity of a MIMO system on large grids.

Bibliography

[1] C. Shannon, "Communication in the presence of noise," *Proceedings of the IRE*, vol. 37, no. 1, pp. 10–21, 1949.

[2] D. Gesbert, M. Shafi, D. Shiu, P. Smith, and A. Naguib, "From theory to practice: an overview of mimo space-time coded wireless systems," *Selected Areas in Communications, IEEE Journal on*, vol. 21, no. 3, pp. 281–302, 2003.

[3] A. Paulraj, D. Gore, R. Nabar, and H. Bolcskei, "An overview of mimo communications-a key to gigabit wireless," *Proceedings of the IEEE*, vol. 92, no. 2, pp. 198–218, 2004.

[4] D. Griffiths and R. College, *Introduction to electrodynamics*. prentice Hall New Jersey, 1999, vol. 3.

[5] S. Choudhary and L. Felsen, "Guided modes in graded index optical fibers," *JOSA*, vol. 67, no. 9, pp. 1192–1196, 1977.

[6] A. Siegman, *Lasers. Mill Valley*. CA: University Science Books, 1986.

[7] F. Byron and R. Fuller, *Mathematics of classical and quantum physics*. Dover Pubns, 1992.

[8] J. Heinrich, E. Zeeb, and K. Ebeling, "Butt-coupling efficiency of vcsels into multimode fibers," *Photonics Technology Letters, IEEE*, vol. 9, no. 12, pp. 1555–1557, 1997.

[9] E. Larsson and P. Stoica, *Space-time block coding for wireless communications*. Cambridge Univ Pr, 2008.

[10] R. Hsu, A. Tarighat, A. Shah, A. Sayed, and B. Jalali, "Capacity enhancement in coherent optical mimo (comimo) multimode fiber links," *Communications Letters, IEEE*, vol. 10, no. 3, pp. 195–197, 2006.

[11] A. Molisch, M. Win, and J. Winters, "Capacity of mimo systems with antenna selection," in *Communications, 2001. ICC 2001. IEEE International Conference on*, vol. 2. IEEE, 2001, pp. 570–574.

[12] D. Gloge, "Optical power flow in multimode fibers," *Bell Syst. Tech. J*, vol. 51, no. 8, pp. 1767–1783, 1972.

[13] R. Olshansky, "Mode coupling effects in graded-index optical fibers," *Applied Optics*, vol. 14, no. 4, pp. 935–945, 1975.

[14] G. Herskowitz, H. Kobrinski, and U. Levy, "Optical power distribution in multimode fibers with angular-dependent mode coupling," *Lightwave Technology, Journal of*, vol. 1, no. 4, pp. 548–554, 1983.

[15] M. Shemirani, W. Mao, R. Panicker, and J. Kahn, "Principal modes in graded-index multimode fiber in presence of spatial-and polarization-mode coupling," *Journal of Lightwave Technology*, vol. 27, no. 10, pp. 1248–1261, 2009.

[16] I. Kimel and L. Elias, "Relations between hermite and laguerre gaussian modes," *Quantum Electronics, IEEE Journal of*, vol. 29, no. 9, pp. 2562–2567, 1993.

[17] K. Appaiah, S. Zisman, S. Vishwanath, and S. Bank, "Analysis of Laser and Detector Placement in MIMO Multimode Optical Fiber Systems," in *IEEE ICC 2012*.

[18] D. Tse and P. Viswanath, *Fundamentals of Wireless Communication*. Cambridge Univ Press, 2005.

[19] K. Appaiah, S. Zisman, A. Das, S. Vishwanath, and S. Bank, "Analysis of Laser and Detector Placement in MIMO Multimode Optical Fiber Systems," in *preparation*.